

OVERVIEW OF HYDROGEN STORAGE TECHNOLOGIES

Brian D. James

Directed Technologies, Inc., 4001 North Fairfax Drive Suite 775, Arlington VA, 22203

Hydrogen is becoming increasingly acknowledged as the energy carrier of choice for the twenty first century. Clean and inexhaustible, substitution of hydrogen for petroleum for use as an automotive fuel would largely eliminate smog in inner cities and health concerns related to air born particulates, and would reduce dependence on foreign oil reserves. Coupled with the high efficiency of Proton Exchange Membrane (PEM) fuel cells as an automotive power plant, simultaneous significant increases in vehicle fuel economy can be made. Indeed, the recent flurry of strategic alliances in the automotive fuel cell world (Ford/Daimler-Benz/Ballard/dbb, General Motors/Toyota) attests to the seriousness with which the automotive industry views fuel cell propulsion, and since fuel cells fundamentally depend on hydrogen fuel, attests to the increasing importance and prominence of hydrogen production, storage, and distribution for the future.

Clearly the hydrogen star is rising. What is less certain is whether the hydrogen bulk supplier community will be able to accommodate the increased consumer demand for hydrogen in the near, mid and far term time frames. The use of liquid hydrocarbons (gasoline, methanol, DME) in onboard reformer fuel cell vehicles is under active development as an interim step to a full hydrogen economy. Such onboard chemical reformation plants capable of converting widely available fuels (gasoline) into a hydrogen rich reformat stream for use by the fuel cell have the major advantage of not requiring major fuel infrastructure alternations. However, creating a load following, highly efficient, compact, low cost reformer is technically challenging and necessarily compromises vehicle system performance compared to a pure hydrogen system. For this reason, onboard hydrocarbon reformation is viewed as an interim link between today's gasoline internal combustion engine automobiles and tomorrows pure hydrogen fuel cell vehicles.

Whether for vehicular onboard storage or stationary bulk storage, the storage of hydrogen has been problematic due to hydrogen's low volumetric density and resulting high cost. This presentation will outline current hydrogen storage techniques for both vehicular and stationary storage and will discuss future hydrogen research trends.

The following methods of hydrogen storage are of interest:

- Liquid hydrogen (LH2)- Liquid hydrogen storage is currently the bulk hydrogen storage medium of choice and has a very impressive safety record. The hydrogen is typically liquefied at the production site in large quantities (10-30 tons per day) and then trucked cross-country in 11,000 gal LH2 tankers with no boil-off losses. Unfortunately, the energy requirements of liquefaction are high, typically 30% of the hydrogen's heating value, leading to relatively high hydrogen cost as compared to gaseous hydrogen. LH2 will likely remain the main technique of bulk, stationary hydrogen storage for the foreseeable future.

Vehicular LH2 systems have the highest H2 mass fractions and one of the lowest system volumes, along with near zero development risk, good fast fill capability, and acceptable safety characteristics. They would appear to be an excellent choice except for two adverse factors: dormancy and infrastructure impact. Dormancy concerns arise due to boil-off losses that will inevitably concern the average car owner, although daily use or proper planning for route or fleet applications can remove most if not all dormancy concerns. Infrastructure impacts are three fold: first, the liquefaction process is costly, second, small scale LH2 production is impractical, and third, low volume distribution/dispensing of LH2 is expensive. Consequently, LH2 systems will not easily support a transition from anemic start-up to a robust H2 economy. Overall, LH2 storage is a most appropriate for a mature H2 economy where the inherent difficulties (and high cost) of large scale remote LH2 production and very small scale LH2 dispensing are least encountered.

- Compressed Gaseous Hydrogen (GH2)- Vehicular compressed hydrogen systems consisting of 34.5 MPa (5,000 psi) gaseous hydrogen in metal or plastic lined, carbon fiber wound pressure vessels offer simplicity of design and use, high H2 fraction,

rapid refueling capability, excellent dormancy characteristics, minimal infrastructure impact, high safety due to the inherent strength of the pressure vessel, and little to no development risk. The disadvantages are system volume and use of high pressure. Integrating the moderate-to-large system volume will clearly challenge the automotive designer, but such a tank volume can be packaged into a "clean sheet" vehicle. In our opinion, the many advantageous features of compressed gas storage outweigh its larger volume. Compressed gas storage is supportable by small-scale H₂ production facilities (on-site natural gas reforming plants, partial oxidation burners, and electrolysis stations) as well larger scale LH₂ production facilities. Thus a plausible H₂ infrastructure transition pathway exists. For these reasons, room temperature compressed gas storage is viewed as the most appropriate fuel storage system for PEM fuel cell vehicles.

For stationary hydrogen storage, GH₂ also offers the advantages of simplicity and stable storage (no boil-off losses) but at a considerably greater volume than LH₂. Even accounting for compression costs, high pressure gaseous hydrogen is cheaper than LH₂. However, except of pipeline transmission, GH₂ lacks the bulk transportability of LH₂. Consequently, GH₂ will mostly be employed for storage of limited hydrogen quantities, for long term storage, or when the cost of liquefaction is prohibitive. Remaining issues for GH₂ include its safety perception, and the current high cost of the pressure vessels and hydrogen compressors.

- **Metal Hydrides-** Metal hydrides can be subdivided into two categories: low dissociation temperature hydrides and high dissociation temperature hydrides. The low temperature hydrides suffer from low H₂ fraction (~2%). The high temperature hydrides require a heat source to generate the high temperature of dissociation (~300°C). Both systems offer fairly dense H₂ storage and good safety characteristics. Indeed it is the bad characteristics of dissociation (high temperature, high energy input) that create the good safety characteristics (no or slow H₂ release in a crash). Overall for vehicular hydrogen storage, metal hydrides are either very much too heavy or their operating requirements are poorly matched to PEM vehicle systems. Without a dramatic breakthrough achieving high weight fraction, low temperature, low dissociation energy, and fast charge time, metal hydrides will not be an effective storage medium for PEM fuel cell vehicles. For stationary storage, the high weight of metal hydride system is not an adverse factor. Consequently, their attributes of high volumetric storage density and stability make them quite attractive. Improving resistance to gaseous contaminants and increasing system cycle life remain as obstacles to overcome.
- **Carbon Adsorption-** Gaseous hydrogen can be adsorbed onto the surface of carbon to attain storage volumetric densities greater than liquid hydrogen. Adhesion capacity is greatly increased by low temperature (particularly cryogenic temperatures) and by high pressure. Indeed significant fractions of the hydrogen contained in carbon adsorbent systems is actually held in gaseous form within the interstitial volume of the carbon adsorbent. Carbon nanofibers are a special type of carbon adsorbent systems which may exploit a fundamentally different mechanism of hydrogen storage and thereby achieve dramatically improved storage capability. However, development and evaluation of nanofibers is at an early stage of development and system characterization is speculative.
- **Microspheres-** Microsphere hydrogen storage systems consists of hollow glass spheres that are "charged" with hydrogen (300°C-500°C, 27-62 MPa for an hour), and discharged by heating (200°C-250°C) and reducing pressure. The microspheres can be pumped or poured from one tank to another, making them viable for vehicular hydrogen storage. Overall, system characterization is immature. Microsphere shelf life remains a concern.

In summary, multiple techniques of hydrogen storage are viable for both vehicular storage and bulk stationary storage. However, no one storage mechanism is ideal. As demand for hydrogen grows, industry must respond by supplying (and storing) hydrogen in ways suitable for the new class of consumers and must educate the public in its safe use.

ANALYTICAL AND EXPERIMENTAL EVALUATION OF PRESSURE VESSELS FOR CRYOGENIC HYDROGEN STORAGE

S. M. Aceves and G.D. Berry
Lawrence Livermore National Laboratory
7000 East Ave., L-641
Livermore, CA 94551, USA
saceves@llnl.gov

ABSTRACT

Insulated pressure vessels are cryogenic-capable pressure vessels that can be fueled with liquid hydrogen (LH₂) or ambient-temperature compressed hydrogen (CH₂). Insulated pressure vessels offer the advantages of liquid hydrogen tanks (low weight and volume), with reduced disadvantages (lower energy requirement for hydrogen liquefaction and reduced evaporative losses).

This paper shows an evaluation of the applicability of the insulated pressure vessels for light-duty vehicles. The paper shows an evaluation of evaporative losses and insulation requirements and a description of the current analysis and experimental plans for testing insulated pressure vessels. The results show significant advantages to the use of insulated pressure vessels for light-duty vehicles.

INTRODUCTION

Probably the most significant hurdle for hydrogen vehicles is storing sufficient hydrogen onboard. Hydrogen storage choices can determine the refueling time, cost, and infrastructure requirements, as well as indirectly influence energy efficiency, vehicle fuel economy, performance, and utility. There are at least three viable technologies for storing hydrogen fuel on cars. These are: compressed hydrogen gas (CH₂), metal hydride adsorption, and cryogenic liquid hydrogen (LH₂), but each has significant disadvantages.

Storage of 5 kg of hydrogen (equivalent to 19 liters; 5 gallons of gasoline) is considered necessary for a general-purpose vehicle, since it provides a 320 km (200 mile) range in a 17 km/liter (40 mpg) conventional car; or a 640 km (400 mile) range in a 34 km/liter (80 mpg) hybrid vehicle or fuel cell vehicle. Storing this hydrogen as CH₂ requires a volume so big that it is difficult to package in light-duty vehicles (Pentastar Electronics 1997), and it certainly cannot be used in freight trucks. The external volume for a pressure vessel storing 5 kg of hydrogen at 24.8 MPa (3600 psi) is 320 liters (85 gal). Hydrides are heavy (300 kg for 5 kg of hydrogen [Michel 1996]), resulting in a substantial reduction in vehicle fuel economy and performance.

Low-pressure LH₂ storage is light and compact, and has received significant attention due to its advantages for packaging (Braess 1996). Significant recent developments have resulted in improved safety (Pehr 1996) and fueling infrastructure (Hettinger 1996). Disadvantages of low-pressure LH₂ storage are: the substantial amount of electricity required for liquefying the hydrogen (Peschka 1992); the evaporation losses that occur during fueling low-pressure LH₂ tanks (Wetzel 1996); and the evaporation losses that occur during long periods of inactivity, due to heat transfer from the environment.

An alternative is to store hydrogen in an insulated pressure vessel that has the capacity to operate at LH₂ temperature (20 K), and at high pressure (24.8 MPa; 3600 psi). This vessel has the flexibility of accepting LH₂ or CH₂ as a fuel. Filling the vessel with ambient-temperature CH₂ reduces the amount of hydrogen stored (and therefore the vehicle range) to about a third of its value with LH₂.

The fueling flexibility of the insulated pressure vessels results in significant advantages. Insulated pressure vessels have similar or better packaging characteristics than a liquid hydrogen tank (low weight and volume), with reduced energy consumption for liquefaction. Energy requirements for hydrogen liquefaction are lower than for liquid hydrogen tanks because a car with an insulated pressure vessel can use, but does not require, cryogenic hydrogen fuel. A hybrid or fuel cell vehicle (34 km/l, 80 mpg) could be refueled with ambient-temperature CH₂ at 24.8 MPa (3600 psi) and still achieve a 200 km range, suitable for the majority of trips. The additional energy, costs, and technological effort for cryogenic refueling need only be undertaken (and paid for) when the additional range is required for longer trips. With an insulated pressure vessel, vehicles can refuel most of the time with ambient-temperature hydrogen, using less energy, and most likely at lower ultimate cost than LH₂, but with the capability of having 3 times the range of room temperature storage systems.

Insulated pressure vessels also have much reduced evaporative losses compared to LH₂ tanks. These results are based on a thermodynamic analysis of the vessels, and are the subject of the next section of this paper.

From an engineering and economic perspective, insulated pressure vessels strike a versatile balance between the cost and bulk of ambient-temperature CH₂ storage, and the energy efficiency, thermal insulation and evaporative losses of LH₂ storage.

THERMODYNAMIC ANALYSIS

The first law of thermodynamics written for a pressure vessel is (VanWylen 1978):

$$M \frac{du}{dt} + M_v \frac{d(c_{p,v}T)}{dt} = Q - \left(\frac{p}{\rho}\right) \dot{m} \quad (1)$$

The two terms in the left-hand side of Equation (1) are the rates of change of the internal energies of the hydrogen and the vessel. Heat transfer into the vessel (Q in the equation) is positive and tends to increase the temperature of the vessel. However, the last term in the right hand side of Equation (1) represents a cooling effect on the vessel, when mass is extracted ($\dot{m} > 0$). Considering that the density of hydrogen is very low, this term is often significant. The last term in Equation (1) is commonly known as the flow work, since it is the work that the hydrogen stored in the vessel has to do to push out the hydrogen being extracted.

Equation (1) is solved for a low-pressure LH₂ storage and for the insulated pressure vessel. The equation is solved iteratively with a computer program which includes subroutines for calculating hydrogen properties. The required property values are obtained from McCarty (McCarty 1975). The specific heat of the vessel materials, $c_{p,v}$ is obtained as a function of temperature from correlations given in the literature (Scott 1967).

VESSEL CHARACTERISTICS

This paper considers three vessels, described as follows:

1. A conventional, low-pressure LH₂ tank with a multilayer vacuum superinsulation (MLVSI) and 0.5 MPa maximum operating pressure.
2. An insulated pressure vessel (24.8 MPa maximum operating pressure) with MLVSI fueled with LH₂.
3. An insulated pressure vessel with microsphere insulation (aluminized microspheres within a vacuum) fueled with LH₂.

Vessel properties are listed in Table 1.

RESULTS

Figure 1 shows hydrogen losses during operation. The figure assumes that the vessels are filled to full capacity (5 kg), and then the vehicles are driven a fixed distance every day. The figure shows total cumulative evaporative hydrogen losses out of a full tank as a function of the daily driving distance. The figure includes information for 17 km/l and 34 km/l cars respectively in the lower and upper x-axes. The figure shows that a low-pressure LH₂ tank loses hydrogen even when driven 50 km per day in a 17 km/l car (100 km in a 34 km/l car). Losses from a low-pressure LH₂ tank grow rapidly as the daily driving distance drops. Insulated pressure vessels lose hydrogen only for very short daily driving distances. Even a microsphere-insulated vessel does not lose any hydrogen when driven 10 km/day or more (20 km/day in the 34 km/l car). Since most people drive considerably more than this distance, no losses are expected under normal operating conditions.

Figure 2 shows losses for a parked vehicle. The figure shows cumulative hydrogen losses as a function of the number of days that the vehicle remains idle. The most unfavorable condition is assumed: the vehicles are parked immediately after fueling. The low-pressure LH₂ tank has 2 days of dormancy (2 days without fuel loss) before any hydrogen has to be vented. After this, losses increase quickly, and practically all of the hydrogen is lost after 15 days. This may represent a significant inconvenience to a driver, who may be unable to operate the vehicle after a long period of parking. Insulated pressure vessels have a much longer dormancy (up to 16 days). Total losses for the insulated pressure vessel with MLVSI is only 1 kg after 1 month of parking. In addition to this, insulated pressure vessels retain about a third of their total capacity even when they reach thermal equilibrium with the environment after a very long idle time, due to their high pressure capacity, therefore guaranteeing that the vehicle never runs out of fuel during a long idle period.

EXPERIMENTAL TESTING AND STRESS ANALYSIS OF INSULATED PRESSURE VESSELS

The analysis presented in this paper has assumed that insulated pressure vessels can be built to withstand the thermal stresses introduced when an initially warm vessel is filled with LH₂. It is desirable to use commercially-available aluminum-lined, fiber-wrapped pressure vessels to avoid the cost of custom-made vessels, even though commercially-available pressure vessels are not designed for low-temperature operation. While the applicability of these vessels for LH₂ storage in vehicles has not been demonstrated, an experiment has been carried out (Morris 1986) in which carbon fiber-aluminum and kevlar-aluminum vessels were cycled over a limited number of cycles (17) at LH₂ temperature. The vessels were burst-tested after cycling. The results of the experiment showed that there was no performance loss (no reduction in safety factor) due to cycling. This experiment indicates that it may be possible to use commercially-available fiber-wrapped aluminum vessels for operation at LH₂ temperature and high pressure. However, additional cyclic testing is necessary, because a vehicle requires many more than 17 fueling cycles.

To accomplish the required testing, an experimental setup has been built inside a high-pressure cell. A schematic is shown in Figure 3. The plan consists of running the vessels through 1000 high-pressure cycles and 100 low-temperature cycles. The cycles are alternated, running 10 pressure cycles followed by a temperature cycle, and repeating this sequence 100 times. Liquid nitrogen will be used for low-temperature cycling, and gaseous helium for high-pressure cycling. This test is expected to replicate what would happen to these vessels during operation in a hydrogen-fueled car.

Cyclic testing of the pressure vessels is being complemented with a finite element analysis, which will help to determine the causes of any potential damage to the vessel during low-temperature operation. Finite element analysis is currently under progress. A mesh has been built, and a thermal analysis of the pressure vessel has been conducted. Validation of the finite element analysis will be done by applying strain gages and temperature sensors to the vessel. Cycled vessels will then be analyzed with non-destructive evaluation techniques, and finally they will be burst-tested, to evaluate any reduction in safety factor due to cycling.

Additional work in progress includes the design of an insulation. This is shown in Figure 4, which indicates that an outer jacket will be built around the vessel. This is necessary for keeping a vacuum space, required for obtaining a good thermal insulation with multilayer insulation (MLVSI). As a part of the insulation design, a pressure vessel outgassing experiment is currently being conducted. This is necessary, because an excessive outgassing rate from the pressure vessel material (fiber and epoxy) may result in a loss of vacuum, considerably reducing the performance of the insulation. The insulation design includes access for instrumentation for pressure, temperature, level and strain, as well as safety devices to avoid a catastrophic failure in case the hydrogen leaks into the vacuum space.

The instrumented and insulated vessel will be cycled with liquid hydrogen to test the instrumentation and insulation performance. Testing will be conducted outdoors at a high-explosives facility to avoid the risk of an explosion that may occur as a result of hydrogen venting.

CONCLUSIONS

This paper shows that insulated pressure vessels have good packaging characteristics and thermal performance compared to LH₂ tanks, and also a potential for reduced need for liquid hydrogen. For these reasons, they are considered to be a good alternative for hydrogen storage. The most important results can be summarized as follows:

1. Insulated pressure vessels do not lose any hydrogen for daily driving distances of more than 10 km/day for a 17 km/l energy equivalent fuel economy. Since almost all cars are driven for longer distances, most cars would never lose any hydrogen.
2. Losses during long periods of parking are small. Due to their high pressure capacity, these vessels retain about a third of its full charge even after a very long period of inactivity, so that the owner would not risk running out of fuel.
3. Previous testing has determined the potential of low-temperature operation of commercially-available aluminum-lined wrapped vessels for a limited number of cycles. Further testing will extend the number of cycles to the values required for a light-duty vehicle. Additional analysis and testing will help in determining the safety and applicability of insulated pressure vessels for hydrogen storage in light-duty vehicles.

NOMENCLATURE

$c_{p,v}$	specific heat of the vessel enclosed within the insulation
\dot{m}	mass flow rate of hydrogen extracted from the vessel
M	total mass of hydrogen stored in the vessel
M_v	mass of the vessel enclosed within the insulation
p	pressure
Q	heat transfer rate from the environment into the vessel
t	time
T	temperature
u	specific internal energy of hydrogen
ρ	density of the hydrogen leaving the vessel

ACKNOWLEDGMENTS

Work performed under the auspices of the U.S. Department of Energy by Lawrence Livermore National Laboratory under Contract W-7405-ENG-48.

REFERENCES

- Braess, H.H., and Strobl, W., 1996, "Hydrogen as a Fuel for Road Transport of the Future: Possibilities and Prerequisites," Proceedings of the 11th World Hydrogen Energy Conference, Stuttgart, Germany.
- Hettinger, W. Michel, F., Ott, P., and Theissen, F., 1996, "Refueling Equipment for Liquid Hydrogen Vehicles," Proceedings of the 11th World Hydrogen Energy Conference, Stuttgart, Germany, pp. 1135-1143.

McCarty, R.D., 1975, "Hydrogen: Its Technology and Implications, Hydrogen Properties, Volume III," CRC Press, Cleveland, Ohio.

Michel, F., Fieseler, H., Meyer, G., and Theissen, F., 1996, "Onboard Equipment for Liquid Hydrogen Vehicles," Proceedings of the 11th World Hydrogen Energy Conference, Stuttgart, Germany, pp. 1063-1077.

Morris, E.E., Segimoto, M., and Lynn, V., 1986, "Lighter Weight Fiber/Metal Pressure Vessels Using Carbon Overwrap," AIAA-86-1504, Proceedings of the AIAA/ASME/SAE/ASEE 22nd Joint Propulsion Conference, June 16-18, Huntsville, Alabama.

Pehr, K., 1996, "Experimental Examinations on the Worst Case Behavior of LH₂/LNG Tanks for Passenger Cars," Proceedings of the 11th World Hydrogen Energy Conference, Stuttgart, Germany.

Pentastar Electronics, 1997, "Direct-Hydrogen-Fueled Proton-Exchange-Membrane Fuel Cell System for Transportation Applications, Conceptual Design Report," Report DOE/CE/50390-9, prepared for U.S. Department of Energy, Office of Transportation Technologies, under contract DE-AC02-94CE50390.

Peschka, W., 1992, "Liquid Hydrogen, Fuel of the Future," Springer-Verlag, Vienna, Austria.

Scott, R.B., 1967, "Cryogenic Engineering," D. Van Nostrand Company, Inc. Princeton, NJ.

VanWylen, G.J., and Sonntag, R.E., 1978, "Fundamentals of Classical Thermodynamics," John Wiley and Sons, New York, NY.

Wetzel, F.J., 1996, "Handling of Liquid Hydrogen at Filling Stations," Proceedings of the 11th World Hydrogen Energy Conference, Stuttgart, Germany, pp. 1123-1134.

Table I. Characteristics of the Hydrogen Vessels Being Analyzed.

	liquid Tank 1	insulated pressure vessels	
		Vessel 2	Vessel 3
Mass of hydrogen stored, kg	5	5	5
Total weight, kg	21	30	30
Internal volume, liters	85	95	95
External volume, liters	112	144	144
Internal diameter, m	0.39	0.42	0.42
Internal surface area, m ²	0.98	1.1	1.1
Aluminum mass within insulation, kg	9	10	10
Carbon mass within insulation, kg	0	10	10
Design pressure, MPa (psi)	0.5 (70)	24.8 (3600)	24.8 (3600)
Performance factor ¹ , m (10 ⁶ in)	-	33000 (1.3)	33000 (1.3)
Safety factor	-	2.25	2.25
Insulating material	MLVSI ²	MLVSI ²	microsphere
Thermal conductivity of insulator, W/mK	0.0001	0.0001	0.0004
Insulation thickness, m	0.02	0.02	0.02
Heat transfer through accessories, W	0.5	0.5	0.5

¹ defined as burst pressure*volume/weight.

² MLVSI = multilayer vacuum superinsulation

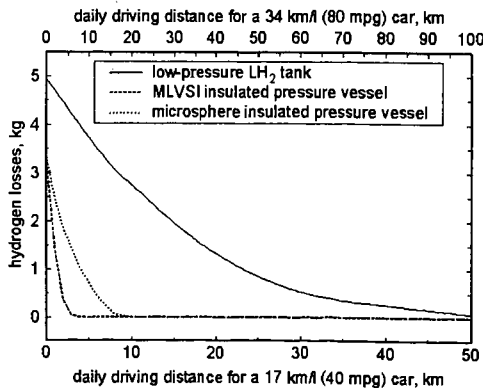


Figure 1. Cumulative hydrogen losses in kg as a function of daily driving distance, for vehicles with 17 km/liter (40 mpg); or 34 km/l (80 mpg) fuel economy, for the three vessels being analyzed in this paper.

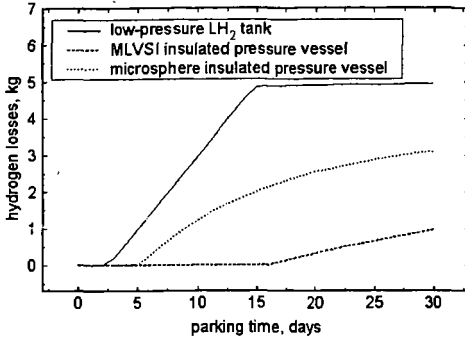


Figure 2. Cumulative hydrogen losses in kg as a function of the number of days that the vehicle remains idle, for the three vessels being analyzed in this paper, assuming that the vessels are initially full.

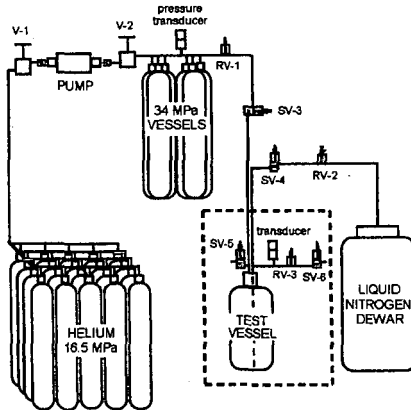


Figure 3. Schematic of the experimental setup for temperature and pressure cycling of a pressure vessel.

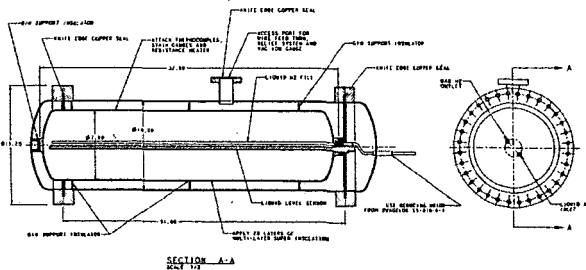


Figure 4. Insulation design for pressure vessel. The figure shows a vacuum space, for obtaining high thermal performance from the multilayer insulation, and instrumentation for pressure, temperature, level and strain.

The Use of Adsorbed Natural Gas Technology for Large Scale Storage.

R.W. Judd, D.T.M. Gladding, R.C. Hodrien, D. R. Bates, J.P. Ingram, M. Allen
BG Technology, Gas Research and Technology Centre, Ashby Road, Loughborough, LE11 3GR, UK

Abstract

Considerable understanding of ANG technology has been gained from work aimed at implementing this method of storage in natural gas vehicles (NGVs). For vehicle applications, maximum gas storage density becomes the ultimate requirement to produce vehicles with an acceptable mileage range. Bulk storage applications require a number of different issues to be addressed relative to vehicle onboard storage, particularly with regard to configuration and physical properties of the adsorbent. A complex compromise of cost versus performance is required which leads to a very different technology configuration than would be expected for vehicles.

1 Introduction

Adsorbed natural gas (ANG) provides a method of storing gas at a substantially higher concentration than can be achieved with simple compression. Although not attaining the density typically found with methods such as LNG, it is potentially much simpler, not requiring the use of refrigeration methods or significant ancillary equipment. Although adsorption on carbon materials developed to date produces its greatest *absolute* enhancement at pressures around 35 bar, higher *relative* gains are obtained in the 3-10 bar range more appropriate to local storage and distribution systems.

Considerable experience of ANG technology has been gained from work on natural gas vehicles (1). For vehicle applications, maximum gas storage density becomes the ultimate requirement, in order to produce vehicles with an acceptable mileage range. To this end, a great deal of research effort has been expended to try and produce active carbons capable of storing up to 190 volumes of gas per volume of storage space (v/v) at pressures of approximately 35 bar. This research has led to the production of some extremely highly engineered carbon materials.

Bulk storage applications require a number of significantly different issues to be addressed in comparison to onboard vehicle storage, particularly configuration, cost and nature of the adsorbent. For bulk storage applications, the viability of the method is critically dependent on the cost of the adsorbing material. Thus although considerable gains can be made in storage capacity by choosing a high performance carbon, the price tends to increase disproportionately to the advantage gained. In addition, high performance carbons tend to have high densities. High density carbons will occupy a smaller volume in the storage vessel; as carbons are priced by weight, there is a proportional rise in cost with increasing density. A compromise in cost/performance is therefore required which leads to a very different choice of carbon for large scale carbon compared to small scale vehicle applications.

This paper will give an overview of work at BG Technology which looks at the feasibility of applying ANG to large scale storage of natural gas

2 The Technical Challenges

Adsorption isotherms in physical chemistry are generally expressed as concentration of adsorbed phase per unit mass of adsorbent. For ANG applications we are concerned with the storage per unit volume. As a result, the density of the adsorbent becomes increasingly important. The storage capacity under these circumstances is usually expressed in terms of volume per volume stored (v/v). This expresses the enhancement in capacity of a particular volume of storage medium relative to an empty container at standard temperature and pressure.

2.1 Carbon development and the adsorption process

Activated carbon is made from cheap natural products such as coconut shells or peach stones. They are subjected to either chemical impregnation followed by heating, or are first pyrolysed to carbon and then subjected to steam treatment. As such they have an extremely high surface area (up to 2500m²/g) and pore sizes as low as 2 nanometres. A typical carbon will be a mixture of small micropores, larger macropores, mesopores from which the gas can escape, and void space. The distribution of these governs the storage capacity of the carbon and is dependent on the preparation

process. The carbon itself can be produced as powder, granules or formed into monoliths or briquettes. Highly activated carbons, and shaped and densified materials have the highest storage capacities, but the increased number of steps required in preparation can push costs per kg very high. Theoretical enhancements of the order of 270 v/v are possible, but practically, the best seen so far are around 150 v/v. Doubling capacity from 75 to 150 v/v at 35 bar can potentially lead to a 20 fold increase in the cost per kg of the carbon. Such monolithic carbons are ideal for vehicle applications where maximum storage capacity is critical and the cost of the carbon is a relatively small part of the overall process. However, as already stated, the excessive cost mitigates against their use for bulk storage. For large scale storage applications, the carbon used is more likely to be in the 80-100 v/v range.

2.2 Deliverability

Any discussion of adsorbed natural gas should make clear that it is not simply the storage capacity of the system which is being considered. *More important is the quantity of gas which can be delivered on desorption.* The storage capacity of an ANG system is always greater than the delivered capacity, usually by around 15%, but sometimes by as much as 30%. The nature of adsorption on microporous systems leads to a large extent of capacity being filled at atmospheric pressure. The amount of gas remaining on the carbon under atmospheric conditions is around 10 times that which would be present in an empty vessel. This gas cannot be discharged from the vessel without reduction in pressure, or displacing it with a more strongly adsorbing gas. The amount of gas which remains in the system is highly dependent on the carbon used. Highly microporous carbons have very steep initial slopes to their uptakes, and therefore retain a larger proportion of the gas on delivery. Careful choice of carbon is necessary to minimize the quantity of retained gas, particularly if use is to be made of ANG in relatively low pressure systems.

2.3 Heat management

The extent of uptake on an adsorbent reduces with increasing temperature, so warming of the system is likely to lead to reduced uptake. Adsorption is of course a process which evolves heat. Due to the highly thermal insulating nature of the carbon material, in a large storage vessel the degree of equilibration of the system with its surroundings is likely to be limited during a typical 8 hour fill. Although filling a completely gas free ANG vessel can produce enough heat to increase temperatures by up to 100°C in a perfectly insulated vessel, it should be borne in mind that in practice this is not the case. At the start of the fill cycle at 0 barg or 1 bara, there is already a layer of adsorbed gas on the carbon, as discussed in the previous section. Adsorption at these initial sites tends to produce the highest heat of adsorption. As anything up to 30% of the total capacity of the bed is present in this non-delivered gas, the total amount of heat released during a typical fill is considerably reduced.

It should also be borne in mind that the total amount of gas stored within a carbon or other adsorbent under pressure is not simply the amount adsorbed in the micropores. This ignores the contribution made by the natural gas in the voids and larger pores where it is stored at the gas phase density of the adopted storage pressure. For a promising carbon, up to 25% of the stored methane can be present as pressurised gas in the voids and therefore contributes no heat of adsorption. Temperature rises of 40-50°C are in fact more likely during a typical fill.

A similar analysis can be used to consider the cooling effect of desorption, where temperatures can drop extensively. The main problem this can cause is in the ease of delivery of the gas at the lowest temperatures, where the rate of desorption will slow.

The experimental programme currently underway indicates that the average carbon temperature is likely to oscillate between -10°C and 40°C, with wall temperatures only varying between 12-25°C. Prevailing environmental conditions during fill and discharge phases are likely to benefit temperature effects during the diurnal phases, as the external temperature is likely to be warmest during delivery of gas when heat is required, and coolest during the fill, when heat is evolved.

2.4 Gas composition

The composition of natural gas varies widely and it always contains gases other than fuel gases, for example, odorant, higher hydrocarbons, CO₂ and N₂. Whereas the adsorption capacity for methane in ANG systems remains constant throughout many adsorption and desorption cycles, such cyclic operation using real natural gas would result in a gradual deterioration of capacity (2,3). This

problems caused by heat transfer during diurnal cycles, and also to issues relating to use of natural gas rather than pure methane. The experimental programme should also allow the tailoring of carbon properties to the requirements of diurnal storage applications, and also allow determination of the ideal internal configuration of the vessel. This latter issue relates particularly to extra methods which may have to be used to cope with problems of heat management.

A development programme was implemented which included parallel experimental work and development of a numerical model.

3.2 The experimental rig

The experimental facility (fig 2) is based around a 500dm³ carbon steel pressure vessel, which has been equipped with 24 positioned thermocouples, internal and external, and 2 internal pressure transducers. The vessel has full bore flanged covers top and bottom and has been designed to allow it to be rotated through 90° to allow measurements to be taken in both upright and horizontal configurations. It is rated up to 40 bar and over a 180°C to -30°C pressure range. Flow into and out of the vessel is controlled using 200dm³/min flow controllers. Temperature, flow and pressure data are continuously logged during experimental runs using a National Instruments 'Labview' based system.

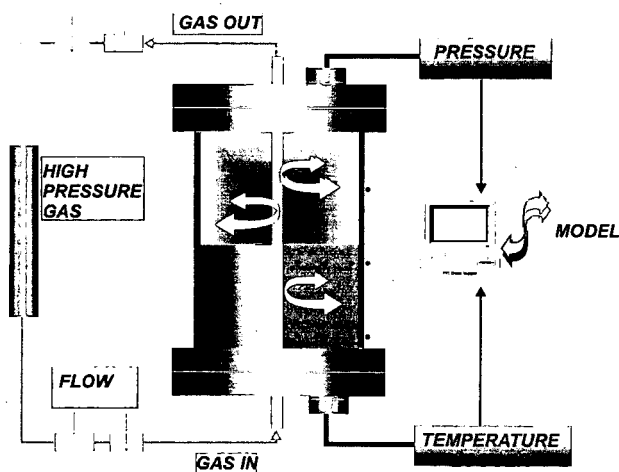


Fig 2. Schematic of experimental rig for cyclic diurnal simulation

3.3 The numerical model

The cylindrical rig has been modelled in its axial and radial dimensions form using a finite difference (explicit scheme) program written in Fortran 90. The model comprises a steel outer shell and a steel inner tube, together with the carbon bed. A single element is assumed to be at equilibrium at a single temperature and the carbon bed pressure is therefore uniform. Conduction is modelled in two dimensions but mass flow (and consequently its associated convective heat transfer) is only allowed in the radial direction. Loading of methane onto the carbon bed, desorption from the bed and the static situation (with no net gain or loss of gas) can be simulated, together with combinations of these phases as is the case in practice. The fit of a simulated run to an experiment involving loading and desorption with a static period in-between is shown in Figure 3.

3.4 Illustrative results

Fig 3 show a subset of data from a simulated diurnal cycle in the 500dm³ vessel, using a commercial carbon material. Only temperature and pressure data are shown here for simplicity. The thermocouples from which these data were obtained were situated in the bulk of the carbon. Close agreement is obtained between experimental and simulated data. Other sets of thermocouples,

deterioration is the result of accumulation of the impurity gases on the adsorbent used because of the preferential adsorption of the heavier hydrocarbon gases.

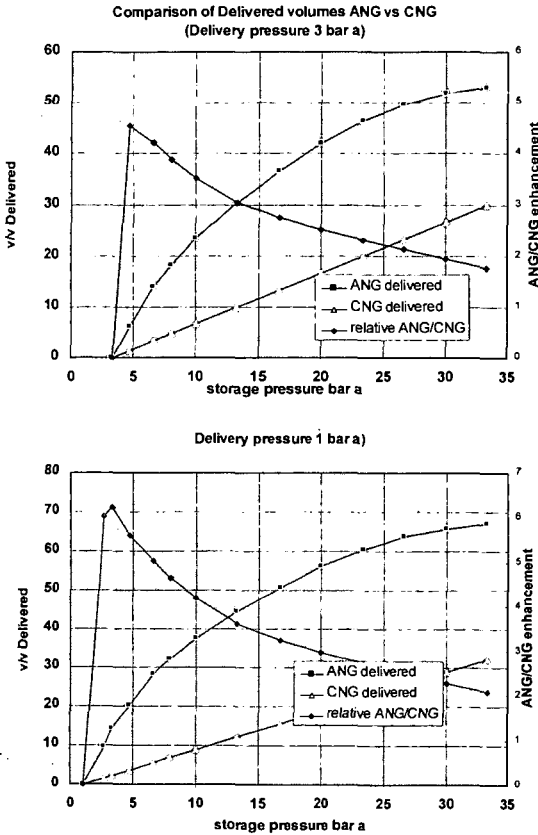


Fig 1. Delivered gas curves for a commercial carbon for different base pressures.

This problem has been addressed in NGV work by the use of some form of preadsorption system to remove the heavier hydrocarbon gases prior to adsorption in the main storage tank. All hydrocarbons adsorb more strongly on carbon than methane, as do the odorants added to natural gas (4,5). One component of natural gas which may require special treatment is water, which although only present at ppm levels in distributed natural gas, tends to adsorb strongly. Experimental work currently under way aims to determine the necessary physical and operating characteristics of a preadsorbing system to protect the main carbon bed.

3 Work in the BG Technology Programme

3.1 Philosophy of work programme

Work is currently underway to estimate the merits of ANG technology for large scale and diurnal storage applications. Techno-economic analyses appeared to indicate that there was a good probability that cost targets for technology use could be met. An experimental programme was initiated to provide predictive data for scale up. These data relate particularly to the extent of any

placed at the vessel core, vessel inner and outer walls and vessel inlet and outlet show corresponding agreement with modelled data. Uptakes of gas were also measured and modelled as a function of time, again with close agreement, but are not illustrated here. The major outcome of this work is the illustration that a real diurnal storage case can be effectively modelled, and current work is extrapolating these data to large scale cases for a variety of practical scenarios.

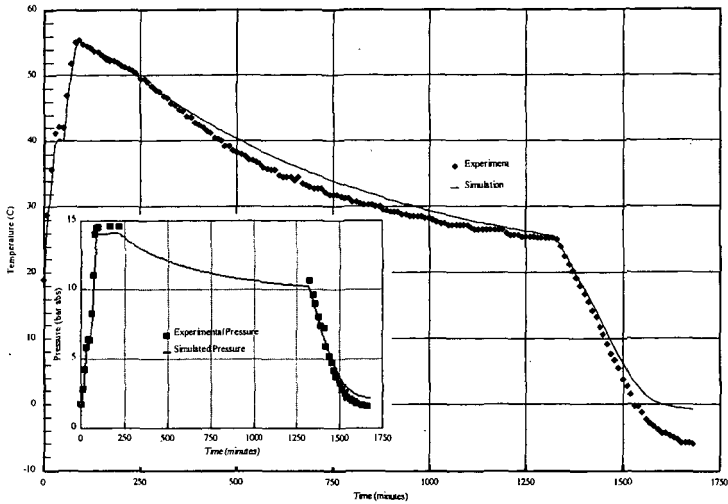


Fig 3. Illustrative data from experimental run and model.

4 Conclusions

The ANG storage method can provide enhancements over pressurisation of the order of 2-10 times depending on storage pressure. Relative gains over pressurisation are greatest at lower pressures, although the absolute amount of gas stored increases with pressure. Delivered rather than stored gas needs to be optimised in order to gain maximum benefit from the technique. The economics of the process depend critically on the choice of carbon adsorbent. Lower density carbons with low cost and high performance are preferred. A compromise between these factors will be required to obtain the most favourable implementation. Adsorbent lifetimes should not be a problem, as long as care is taken to prevent adsorption on the main bed of components which could irreversibly adsorb and degrade performance.

5 References

- 1 C. Komodromos, S. Pearson and A. Grint. The Potential of Adsorbed Natural Gas for Advanced on Board Storage in Natural Gas Fuelled Vehicles. IGRC, Florida, 1992.
- 2 R.W. Judd, C. Komodromos and D.W.J. Jack. Adsorbed Natural Gas: The Potential For Bulk Storage. Internal BG report.
- 3 A. Golvoloy and E.J Blais, SAE Conference Proc., Pittsburgh p 47 (1983).
- 4 A.L Chafee, H.J Loeh, and A.G Pandolfi Methane Adsorption on High Surface Area Carbons. CSIRO, Report FT/IR 031R (1989).
- 5 J.A. Ritter and R.T. Yang, Ind. Eng. Chem. Res. 26 1679 (1987).

6 Acknowledgements

The authors would like to thank BG plc for permission to publish this paper, and also Dr R.E. Critoph of Warwick University for extensive input into the production of the numerical model.

CARBON MOLECULAR SIEVES DERIVED FROM POLYMERS FOR NATURAL GAS STORAGE

C. H. Chang* and A. Stella**, AlliedSignal Inc.
*Des Plaines, IL 60017 & **Morristown, NJ 07962

ABSTRACT

In the last several years, advances have been made in the development of adsorbents for the storage of natural gas. At AlliedSignal, we have focused on the polymer-derived carbon molecular sieves for the control of micropore size, micropore volume, bulk density, and packing efficiency to enhance storage capacity. A deliverable storage efficiency of 150 volumes of methane per volume of adsorbent has been achieved at a storage pressure of 500 psig. This presentation will discuss the synthesis of the materials and the preparation and characterization of the advanced carbon molecular sieves. Structural parameters and storage capacities of these carbon molecular sieves will be compared with other carbonaceous materials. In addition, theoretical studies on determining optimum pore sizes for methane storage and molecular simulations of isotherms and isosteric heats will be presented for comparison with our carbon molecular sieves.

1. INTRODUCTION

Storage of natural gas with an adsorbent has been considered a promising technology for the on-board storage of natural gas for vehicular applications^{1,2}. Among adsorbents investigated, carbon materials are most effective in the storage of natural gas at low pressures (e.g. 300-500 psig)³. Critical issues in the commercialization of the adsorbed natural gas storage technology include the storage capability of the adsorbent and the ease and cost of its manufacture.

The objective of the present study is to develop a high capacity carbon adsorbent which can be commercially produced at a reasonable cost. In the course of the study, molecular modeling and simulation efforts, similar to those reported by Matranga, Stella, Myers and Glandt⁴, were conducted to help in the design and optimization of the pore structure of the carbon adsorbent for the storage of natural gas.

2. EXPERIMENTAL AND RESULTS

2.1 Adsorption Theory and Development of Carbon Molecular Sieves

The adsorbents developed in this study are all variants of activated carbon molecular sieves developed by AlliedSignal Inc. The development involved first understanding the theoretical basis for adsorption followed by experimentation to achieve material properties suggested from the theoretical results.

Molecular modeling and simulation were used in the optimization process for these sorbents. An understanding of the potential energy functions between methane and the carbon surface was applied to pore size control. Calculation of the second virial coefficients for adsorption, B_{1S} , as a function of graphitic carbon slit width, was performed by numerical integration of the gas-solid potential over the pore volume⁵. The maximum second virial coefficient lends insight into the optimal slit width for methane adsorption. Slits that are too large have too small a B_{1S} , due to a lack of cooperative interaction between the adsorbate and both walls of the slit. This means that the attractive forces are too small due to the large dimensional width of the pore. At too small a pore width, the repulsive forces become too large for effective adsorption. The calculation showed an optimal slit pore width of 11.4 Å for methane adsorption.

Using the information from the second virial coefficient study, carbon sorbents were prepared from a proprietary polymer through a multi-step process. The carbon molecular sieve (CMS) materials were synthesized by carbonization of a proprietary polymer followed by activation with a gaseous stream to develop optimal pore structure. *Figure 2* shows a comparison of pore structures for various activated CMS materials.

The slit model and a more complex strip models which includes both structural and chemical heterogeneity were applied in order to investigate isotherms and isosteric heats of adsorption. Grand Canonical Monte Carlo (GCMC) simulations were performed. Isotherms and isosteric heats of adsorption were calculated from the fluctuations in the number of molecules and energy⁶. Figure 3 shows a heterogeneous surface of the strip model reduces the adsorption amount as compared to the homogeneous slit model. Figure 4 shows that the heterogeneous materials have isosteric heats that decrease with the coverage due to occupation of lower energy adsorption sites as coverage increases. The theoretical work shows that homogeneity of the material will enhance adsorption greatly.

2.2 Preparation and Evaluation of Carbon Molecular Sieves

The preparation of the polymer-derived carbon molecular sieves consists of four basic steps: preparation of the polymer precursor, pelletization or shaping of the precursor, carbonization, and activation of the resulting carbon molecular sieve. For the development of a high capacity adsorbent for natural gas storage, all these four process steps are investigated and optimized for volumetric storage efficiency.

2.2.1 Precursor Synthesis: A number of polymeric materials were initially screened for the ability to form microporous carbon structures with proper pore size/ pore distribution and with high carbon yield. Results of this study showed very conclusively that only a small number of polymer candidates are potentially promising. These materials include polyvinylidene chloride (PVDC), polyvinylidene fluoride, polyacrylonitrile, polychlorotrifluoroethylene, and phenolic resins. Copolymers incorporating these monomers are also potentially effective. Among these potential precursor materials, we chose to focus on the PVDC system.

Not only is the chemical nature of the monomer important but also the physical chemical properties of the polymer material. The effects of polymer molecular weight, polymer particle size and size distribution, and the density of the polymer particle were extensively studied. Synthesis method, initiation catalyst and polymerization temperature are all critical in the synthesis of the best precursor⁷.

2.2.2 Pelletization and shaping of the precursor: Parameters that were found to be important for the synthesis of the adsorbent for natural gas storage are pellet configuration, pellet piece density and the uniformity of the void space throughout the pellet. During the pelletization of PVDC precursors, there were no shape additives since this may cause decreases in the volumetric/gravimetric efficiency of the resulting CMS.

2.2.3 Carbonization of the Pellet during Thermal Transformation: The PVDC precursor goes through softening, decomposition, and carbon structure formation at various temperatures. The formation of the pore structure and the density of the resulting adsorbent are critically determined by the temperature program used for the precursor pellet. Of particular importance is the fact that the PVDC precursor loses 50% of its total HCl at about 200°C and the rest of the HCl at about 500°C. The control of the kinetics of HCl evolution determines the pore size of the resulting CMS and the packing density of the adsorbent for natural gas storage.

2.2.4 Activation: The volumetric efficiency of the natural gas adsorbent is optimized by increasing the gravimetric efficiency and maintaining high packing density of the adsorbent through activation. Oxidizers such as carbon dioxide, air, and steam, and their combinations were investigated. The activation process increases the total micropore volume and modifies the pore size and pore distribution. Differences in the activation process are illustrated in Table 1.

2.2.5 Evaluation of the activated CMS: The storage efficiency of the activated carbon molecular sieves was evaluated gravimetrically. The adsorbent material was packed in a 40 mL test cell. The material was heated at 150°C under vacuum (less than 25mTorr) for a period of greater than 2 hours. Methane gas was used throughout the study to simulate the natural gas storage. The methane is introduced to the test cell at 25°C at various

pressures and the amount of methane stored was determined by weight uptake at equilibrium. The total volumetric gas storage delivery was calculated by using the total amount of methane stored per unit volume less the methane volumetric density at the delivery condition of 746 mmHg and 26.3°C, which is 0.000643 g/mL. The V/V value was determined by dividing the total deliverable gas volume with the volume of the empty test cell which was volumetrically calibrated with methane. Results of the storage measurements at 300 psig are summarized in Table 2 for comparisons with other carbon adsorbents.

2.2.6 Improvement of Storage Capacity by Packing: As shown in Table 2, the volumetric efficiency of ACMS for methane storage is affected by the packing density of the adsorbent material. A packing technique employing at least two sizes of adsorbent particles having nominal diameters differing by at least 7:1 was developed⁸. Table 3 illustrates the improvement of deliverable V/V capacity with a binary packing system.

3. CONCLUSION

Through careful screening and parametric process optimization, a class of activated carbon molecular sieves has been developed for the on-board storage of natural gas. A deliverable volumetric capacity of 150 V/V has been achieved at 500 psig. The commercialization of this class of adsorbent depends on the market need. Further studies are required to further improve the efficiency and economics of the adsorbent.

REFERENCES

1. J. Wegrzyn, H. Weismann, and T. Lee, Low Pressure Storage of Natural Gas on Activated Carbon Proceedings: Annual Automotive Tech. Develop, Dearborn, MI (1992).
2. C. R. Nelson, Physical Sciences NGV Gas Storage Research, Gas Research Institute, Chicago, IL (1993).
3. D. F. Quinn, J. A. McDonald, and K. Sosin, 207th ACS National Meeting, San Diego, CA (1994).
4. K. Matranga, A. Stella, A. Myers, and E. Glandt, Sep. Sci. and Tech. (1992) **27**, 1825-1836.
5. A. Stella, "Adsorption on Activated Carbon: Comparison of Molecular Simulation with Experiment", Ph.D. Thesis, University of Pennsylvania, 1993.
6. D. Nicholson, N. G. Parsonage, "Computer Simulation and the Statistical Mechanics of Adsorption", Academic Press, London, 1982.
7. C. H. Chang, and G. J. Seminara, "Preparation of Hydrophobic Carbon Molecular Sieves", U. S. Patent #4,820,681, April 11, 1989.
8. C. H. Chang, "Packing Adsorbent Particles for Storage of Natural Gas", U. S. Patent #5,308,821, May 3, 1994.

Table 1. The Effect of Activation on the Properties of PVDC-derived CMS

Sample #	Activating gas	Activation condition (°C)	Yield after activation (%)	Packing density (g/mL)	BET surface area (m ² /g)	Micropore volume (mL/g)
1	None	None	100	0.633	1484	0.45
2	Steam	825	65.8	0.435	1861	0.56
3	Steam	850	25.0	0.240	2280	1.82
4	CO ₂	800	73.0	0.469	1864	0.56
5	CO ₂	854	21.4	0.559	2145	0.65

Table 2. Storage Efficiency of Activated CMS for Methane at 25°C and 300 psig

Carbon Adsorbent	Packing density (g/mL)	Storage temperature (°C)	Gravimetric efficiency (g/g)	Volumetric efficiency (V/V)
Norit carbon	0.387	24	0.1138	69
Calgon PCB	0.445	23	0.1095	76
Calgon PCB	0.500	27	0.0108	79

-Continued (Table 2)

Nuchar WV-B	0.259	25	0.1142	46
Anderson AX-21	0.355	25	0.1569	87
Saran carbon	0.320	25	0.070	51
CMS-1	0.633	25	0.1031	112
ACMS-1-1	0.545	25	0.133	122
ACMS-1-2	0.544	25	0.1401	128
ACMS-1-3	0.492	25	0.1363	115
CMS-2	1.022	25	0.1001	158
ACMS-2-1	0.837	25	0.1334	173

Table 3. Storage Efficiency of Activated CMS Systems with Binary Packing

Adsorbent	1	2	3	4
Particles	2.3mm pellet	2.3mm pellet/beads	1.6mm pellet	1.6mm pellet/beads
Test cell (mL)	39.89	39.89	39.60	39.60
Pellet wt.(g)	21.08	21.02	21.41	21.44
Beads wt.(g)	-	5.74	-	5.43
Total dry wt (g)	20.72	26.23	21.05	26.33
Packing density (g/mL)	0.519	0.658	0.532	0.665
CH ₄ adsorbed (g/g) @ 0psig	0.65	0.77	0.61	0.79
100	2.12	2.64	2.14	2.62
200	2.78	3.43	2.82	3.38
300	3.28	3.89	3.29	3.88
400	3.61	4.22	3.63	4.24
500	3.88	4.54	3.89	4.56
600	4.12	4.79	4.13	4.80
700	4.32	4.95	4.37	4.99
800	4.51	5.16	4.53	5.16
900	4.68	5.32	4.70	5.32
Deliverable V/V @ 0 psig	0	0	0	0
100	57.33	72.92	60.11	71.89
200	83.06	103.73	86.82	101.75
300	102.56	121.67	105.28	121.39
400	115.43	134.54	118.64	135.53
500	125.96	147.02	128.28	148.10
600	135.32	156.77	138.28	157.53
700	143.12	163.01	147.71	164.99
800	150.53	171.20	153.99	171.69
900	157.16	177.44	160.67	177.96

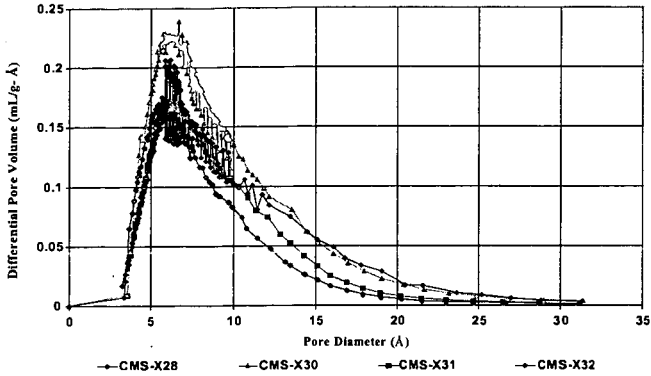


Figure 2 Horvath-Kawazoe Plot for pore structure of CMS materials

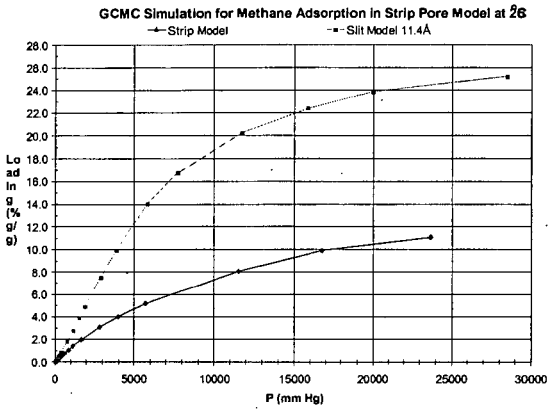


Figure 3. GCMC Simulation for Methane Adsorption in Strip Pore Model at 25°C

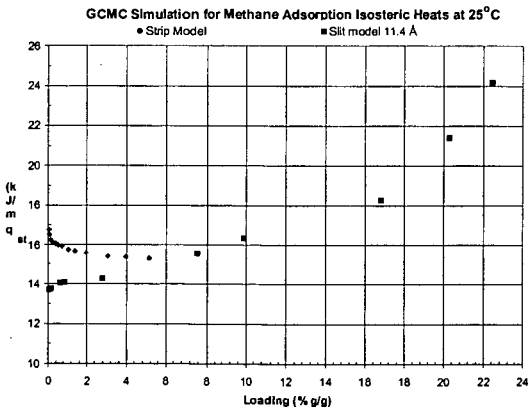


Figure 4. GCMC Simulation for Methane Adsorption Isothermic Heats at 25°C

GAS-STORAGE CARBONS PREPARED BY ALTERNATING OXYGEN CHEMISORPTION AND THERMAL DESORPTION CYCLES

Marek A. Wójciewicz, Brian L. Markowitz, Girard A. Simons*, and Michael A. Serio

Advanced Fuel Research, Inc., 87 Church Street, East Hartford, CT 06108-3742
*Simons Research Associates, 3 Juniper Road, Lynnfield, MA 01940-2416

Keywords: gas storage, activated carbon, chemisorption, desorption

ABSTRACT

The desirable characteristics of activated carbons for gas-storage applications are: (1) high microporosity (pores smaller than 2 nm); and (2) low voidage in the storage container (e.g., the use of shaped sorbent elements). A transient chemisorption-desorption char activation technique was used to maximize micropore formation and minimize mesoporosity. Several carbons were prepared at different degrees of burn-off, and the BET surface areas were found to be up to 2000 m²/g. The carbons were prepared in the form of pellets to show that the future use of shaped elements can lead to the reduction of voidage in the storage container by up to 40%. The adsorption isotherms of the produced carbons showed high microporosity and no appreciable mesoporosity, even at high burn-offs.

INTRODUCTION

Gas storage by adsorption on activated carbon is possible at relatively low pressures using activated carbons with a well developed microporosity, i.e., with pores whose radius, r_p , is less than $r_{\text{lim}} \cong 10 \text{ \AA}$. The generation of microporosity requires a uniform surface phenomenon, such as steady-state gasification in the limit of kinetic control or an alternating adsorption-desorption process in which a reactant gas is chemisorbed on the active sites of a carbon surface and then allowed to desorb, removing the carbon from the walls of the pores [1,2]. A model was presented [3] to describe pore growth in microporous carbons and was used to relate the potential micropore volume to the characteristics of the starting material (initial char). Modeling results show that the microporosity can be maximized by choosing an initial char with minimum initial open porosity and significant initial blind porosity within angstrom-size pores. As a spatially uniform surface recession may be obtained via char gasification in the limit of kinetic control, the microporosity-evolution model [3] has been coupled to a pore structure/pore-transport model [4] capable of describing the simultaneous action of diffusive and kinetically-controlled processes. The integrated model [5] was used to determine the conditions under which diffusion-control may be avoided and the char microporosity maximized. Predicted steady-state activation times are extreme for millimeter-size particles (10⁴ hours), and faster processes are sought. One such process is that of alternating oxygen chemisorption and desorption [1,2]. Rapid adsorption of oxygen onto the char surface in the absence of desorption (via low-temperature chemisorption), followed by rapid high-temperature desorption in the absence of oxygen, may be used to cyclically remove carbon from the walls of the pores.

In this paper, theoretical analysis of the cyclic chemisorption-desorption process is carried out to assess the time scales of: (1) the oxygen chemisorption step; and (2) the thermal desorption of surface oxides. In addition to the results of the modeling effort, microporosity evolution is reported for chars prepared using the above activation technique.

MATERIALS AND EXPERIMENTAL TECHNIQUES

A sample of granular polyvinylidene chloride (PVDC), provided by Solvay Polymers, Inc., Houston, Texas, was used as a carbon precursor. PVDC was first pressed into pellets, using a ten-ton press, and then subjected to carbonization. The initial dimensions of the pellets were 13 mm in diameter and ~5 mm in thickness, and the initial weight of each pellet was approximately one gram. The PVDC-carbonization procedure consisted of the following steps: (1) heating from room temperature to 170 °C at 5 °C/min; (2) heating to 230 °C at 0.1 °C/min; (3) heating to $T_f = 900 \text{ °C}$ at 2 °C/min; (4) holding at T_f for time $\tau_f = 240 \text{ min}$; and (5) cooling down to room temperature at ~22 °C/min. After carbonization, the samples were activated to the desired degree of burn-off using a thermogravimetric analyzer (TGA), and the following routine was performed cyclically: (1) purging the system at 200 °C for 17 minutes in helium; (2) heating at 100 °C/min to $T_a = 900 \text{ °C}$ (He); (3) holding for 5 minutes (He); (4) cooling at ~22 °C/min to $T_{\text{ch}} = 200 \text{ °C}$ (He); and (5) switching from the flow of helium to oxygen and holding for $\tau_{\text{ch}} = 15 \text{ minutes}$ in O₂. At specified levels of burn-off, samples were taken out of the TGA, weighed, and nitrogen adsorption isotherms were determined using a Micromeritics Digisorb 2600 analyzer.

RESULTS AND DISCUSSION

Modeling of the Kinetics of Oxygen Chemisorption and Surface-Oxide Desorption

The primary limitation of the adsorption process is the time required for oxygen to reach the smallest pores in the char. The high chemisorption rate will generate large oxygen gradients within the particle, but diffusion along these gradients is still responsible for delivering the oxygen to the smallest pores. A model has been developed to describe this transient chemisorption process. A chemisorption "front", coupled with gas-phase diffusion, progresses into the pore structure and deposits chemisorbed oxygen on carbon active sites. This model has been used to determine the time required for complete chemisorption of oxygen onto the walls of the smallest pores.

For phenol-formaldehyde char, chemisorbed oxygen loadings of the order of 12 mg O₂/g C were obtained at 300 °C in one atmosphere of oxygen [6]. The chemisorption time was about 80 minutes, the BET surface area of the char was about 400 m²/g C, and the char particle diameter was of the order of 100 microns. A primary concern is how the chemisorption time scales with particle size and oxygen partial pressure. The model described above has been used to predict this scaling. If s_p represents the internal surface area of the carbon (m²/g C), and σ_w represents the chemisorbed oxygen loading per unit surface area (g O₂/m²), then $s_p\sigma_w$ is the chemisorbed oxygen loading in g O₂/g C. Oxygen loadings of the order of 12 mg/g and an internal surface area of 400 m²/g are consistent with surface loadings (σ_w) of 3×10^{-9} g/cm². Using this set of chemisorption parameters, model predictions for the chemisorption times are illustrated in Figure 1. In the limit of kinetic control (small particles), increased gas pressure significantly reduces the chemisorption time. However, in the limit of diffusion control (large particles), increased gas pressure does not enhance diffusion. It is clear that operating in one atmosphere of oxygen on up to 7 mm particles will maintain chemisorption times of the order of one hour.

The desorption process is just the reverse from the adsorption process. A desorption "front," coupled with gas phase diffusion and viscous convection, progresses into the pore structure and desorbs the oxygen from the carbon active sites. As the particle temperature is raised, the internal gas pressure increases and viscous convection of the gas from the pore structure becomes rate limiting. This is illustrated in Figure 2. Internal gas pressures in excess of a few hundred pounds per square inch are sufficient to create desorption times less than one tenth of an hour per cycle for centimeter-size particles. As the desorption temperature, and therefore pressure, may be arbitrarily increased, the alternating chemisorption-desorption process is readily limited by the chemisorption step. As each chemisorption-desorption cycle will chemisorb only ~12 mg O₂/g C, and desorption will remove only 9 mg carbon per gram of carbon, up to 100 cycles may be required to fully activate the carbon. As temperature cycling may require less than one hour per cycle, it is apparent that this activation process is much faster than kinetically controlled gasification and may be used to activate particles up to one centimeter in diameter on time scales of the order of 100 hours.

Preparation and Characterization of Gas-Storage Carbons

An important consideration in gas-storage applications is the degree of sorbent packing within the storage container. To achieve maximum volumetric storage density, the voidage in the container needs to be minimized. Although some amount of voidage is desirable to ensure adequate gas transport within the sorbent-filled container, the 30-40% voidage typical of randomly packed particles is excessive. Thus, an ideal gas-storage system would consist of a nearly 100% microporous sorbent in the form of tightly packed, shaped elements, e.g., discs 5-10 mm in thickness.

The traditional char-activation methods, which are based on steady-state carbon gasification, usually lead to pore-mouth widening and to the creation of the undesirable mesoporosity. The problem is caused by mass-transfer limitations that occur within the char particle, and this phenomenon is increasingly more severe for particles of larger sizes. Thus, the steady-state activation methods are incapable of producing large elements of highly microporous sorbent. This is in contrast to the cyclic chemisorption-desorption method, which, by obviating the mass-transfer limitations, should allow to obtain large elements of microporous sorbent. This presumption is tested below by analyzing the pore structure of sorbent pellets activated using the cyclic method.

Adsorption isotherms of the PVDC char pellets activated to different burn-offs are shown in Figure 3. It is evident that all the curves have the shape of a Type I isotherm, which is characteristic of highly microporous materials [7]. It is remarkable that even the pellets with as much as 87% burn-off do not show mesopore formation (transition to a Type IV isotherm).

Although the BET surface-area analysis is not quite applicable to highly microporous materials [7], the results can nevertheless serve as an index of sample microporosity. In other words, BET surface areas reported for microporous solids will not have physical meaning, but larger values will indicate a higher degree of microporosity. Another measure of microporosity is the micropore volume evaluated using the Dubinin-Radushkevich equation [8,7]. BET surface areas and micropore volumes of the PVDC char pellets are presented in Figure 4. It can be seen that both variables increase with the increasing burn-off, which indicates that the sorbent becomes more and more microporous as activation progresses.

Additional insights into the morphology of sorbent pellets can be provided by Scanning Electron Microscopy (SEM). SEM pictures of an activated PVDC char pellet are shown in Figure 5. It can be seen the PVDC granules that were initially present within the pellet have changed their original spherical shape (uncompressed PVDC polymer) to a more pentagonal or hexagonal pattern (PVDC char pellet). These particles have an approximate size of 170 microns. The change in particle shape drastically decreases the ~40% voidage typically found in spherical particles. Another interesting observation is the 5-10 micron spaces between individual granules within each pellet. It is expected that these spaces will make gas transport into and out of the storage container far less restricted than in the case of "solid" pellets. Preliminary calculations carried out for the above material show that mass transfer within a bed of shaped sorbent elements should not be a serious problem for gas-storage applications. A more detailed analysis of this result will be discussed in a future publication.

Figure 5 also shows one-micron pits, which are most likely formed during the evolution of pyrolysis gas. Modifications in the PVDC pyrolysis routine may lead to a change in the size and the number of these structural features.

CONCLUSIONS

- Theoretical analysis of the cyclic chemisorption-desorption process shows that char particles up to one centimeter in size can be activated on time scales of the order of 100 hours.
- All PVDC-derived carbons, activated to burn-offs of up to 87% using the cyclic technique, were found to exhibit Type I adsorption isotherms. This is indicative of a high degree of microporosity. Nitrogen BET surface areas and Dubinin-Radushkevich micropore volumes were found to be up to 2000 m²/g and 0.84 cm³/g, respectively. It can be concluded that the concept of producing large, shaped elements of microporous carbon has been experimentally validated. This finding is associated with the benefit of an increased volumetric storage density (by up to 40%) due to improved sorbent packing. First tests of hydrogen-storage capacity of the above sorbents have been carried out, and the results look very encouraging [2].
- SEM micrographs show that sorbent pellets are composed of nested pentagonal or hexagonal particles about 170 μm in size. Spaces between the particles are 5–10 μm wide, and they should provide a good medium for hydrogen transport without creating excessive voidage.

ACKNOWLEDGMENTS

This research was supported by the NASA Johnson Space Center under SBIR contract No. NAS9-19470. The authors also acknowledge helpful comments contributed by Dr. David F. Quinn of the Royal Military College of Canada and Professor Eric M. Suuberg of Brown University.

REFERENCES

- 1 Quinn, D. F. and Holland, J. A., U.S. Patent No. 5,071,820, 1991
- 2 Wójtowicz, M. A., Smith, W. W., Serio, M. A., Simons, G.A. and Fuller, W. D., in *Carbon '97* (Ext. Abstr. 23rd Biennial Conf. Carbon), The Pennsylvania State University, State College, PA, 1997, vol. I, pp. 342-343
- 3 Simons, G. A. and Wójtowicz, M. A., in *Carbon '97* (Ext. Abstr. 23rd Biennial Conf. Carbon), The Pennsylvania State University, State College, PA, 1997, vol. I, pp. 328-329.
- 4 Simons, G.A., in *Nineteenth Symposium (International) on Combustion*, The Combustion Institute, Pittsburgh, PA, 1982, pp. 1067-1076.
- 5 Simons, G. A. and Wójtowicz, M. A., in *Proc. 9th Int. Conf. on Coal Science*, DGMK, Hamburg, Germany, 1997, pp. 1783-1786.
- 6 Wójtowicz, M. A., *Thermogravimetric Study of Active Sites in the Process of Low-Temperature Oxidation of Char*, Ph.D. thesis, Brown University, Providence, RI, 1988.
- 7 Gregg, S. J. and Sing, K. S. W., *Adsorption, Surface Area and Porosity*, Academic Press, London, 1982.
- 8 Dubinin, M. M. and Radushkevich, L. V., *Proc. Acad. Sci. USSR* **55**, 331, 1947; Dubinin, M. M., *Russ. J. Phys. Chem.* **39**, 697, 1965.

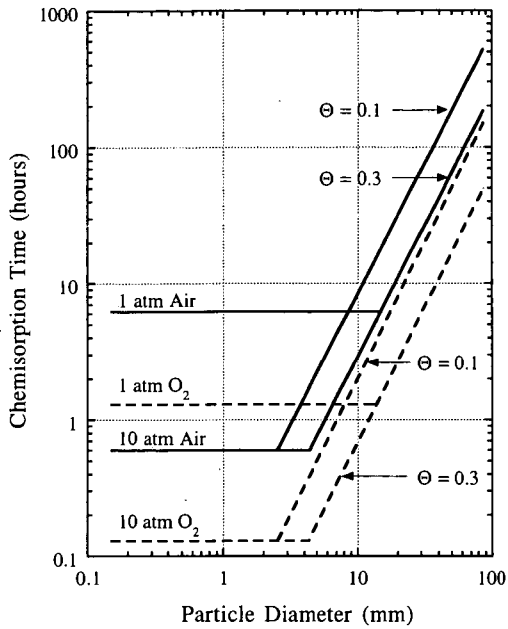


Figure 1. Scaling of chemisorption time with particle size and gas pressure (phenol-formaldehyde resin char carbonized at 1000 °C for 2 hours; Θ is char porosity).

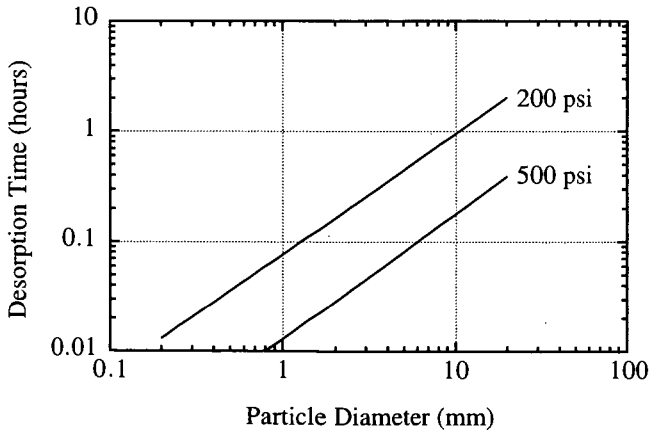


Figure 2. Scaling of desorption time with particle size and internal gas pressure (convection limited, 200 psi and 500 psi).

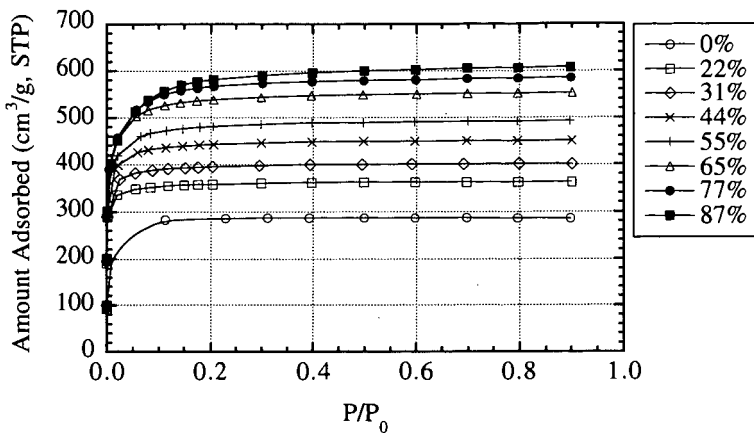


Figure 3. Nitrogen adsorption isotherms for PVDC-char pellets activated to various degrees of burn-off.

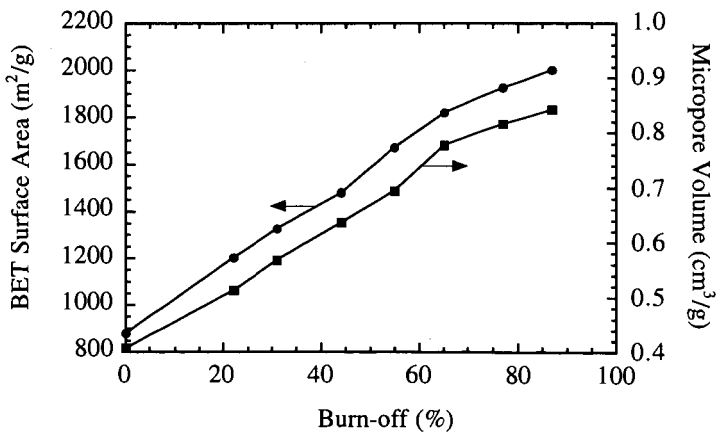


Figure 4. Nitrogen BET surface area and Dubinin-Radushkevich micropore volume versus per cent burn-off for PVDC char pellets.

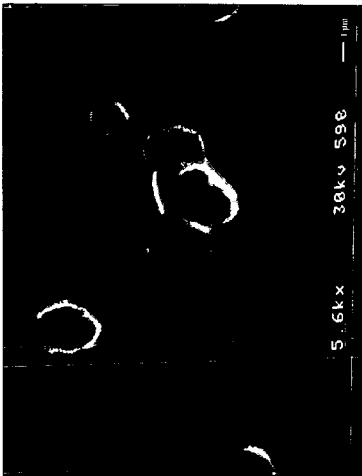
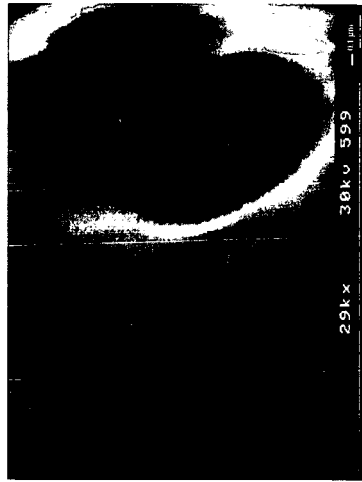
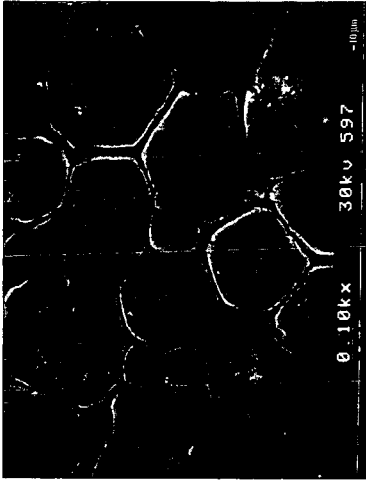


Figure 5. SEM micrographs of a PVDC char pellet ($T_i = 905^\circ\text{C}$, $\tau_i = 5\text{ min}$, $T_{ch} = 200^\circ\text{C}$, $\tau_{ch} = 15\text{ min}$, $T_d = 900^\circ\text{C}$, $BO = 64\%$).

CH₄ STORAGE ON COMPRESSED CARBONS

Aurora M. Rubel and John M. Stencil
Center for Applied Energy Research, University of Kentucky, Lexington, KY 40511

ABSTRACT

The uptake of CH₄ in three commercially-produced carbons before and after physical and chemical modification were studied using a specially designed cell within a high pressure TGA. The uptake capacities in non-compacted and compacted carbons and their pore size distributions were compared. After compaction, a carbon having 75-38 μ m particles adsorbed more CH₄ than the same carbon having larger particles of 1700-425 μ m even though the resultant density of the later sample was greater. Compaction of graphite powder produced significant microporosity, imparting capacities of 25 ml CH₄ at STP/ml carbon. Even though greater microporosity in carbons increases CH₄ storage capacities, high microporosities usually leads to low piece densities and difficulties during compaction. Hence, methods to improve piece density while maintaining CH₄ capacities were investigated. One method involved the mixing a highly microporous carbon with graphite and then compacting the mixture. A blend of 75:25 by volume (carbon : graphite) contained the same adsorption capacity on a volume CH₄/volume carbon basis as did the pure carbon sample; the blend had better compaction properties. Another method involved chemical deposition on and within the carbon. Diethylsilane was impregnated on and in a highly microporous carbon resulting in greater piece density and increased CH₄ uptake capacity.

INTRODUCTION

The commercial utilization of microporous carbons to store natural gas at low pressures will require the optimization of many factors including: maximizing the pore volume around 1.1 nm¹; minimizing adsorption/desorption cycle times²; and, increasing the volume-per-volume (v/v) storage capacities, i.e. volume of CH₄ stored-per-volume of carbon used. Optimization and production of suitable carbons has been studied by several researchers³⁻⁶. In transportation applications, the CH₄ sorbent will ultimately need to be contained within a fixed volume, thereby requiring relatively high densities which produce desirable v/v storage capacities.

Previous work has shown that treating activated carbons with surfactants can improve their compressibility and reduce the work needed for densification⁷. However, the CH₄ storage capacities of these carbons were not determined. The present study investigated changes in the compressibility and CH₄ uptake of microporous carbons when physical modifiers were added before compaction.

EXPERIMENTAL

The compaction properties of three carbons and their CH₄ uptake were studied. Three commercially-made carbons, including Barnebey-Sutcliffe A207 (two particle size fractions, 75-38 μ m and 1700-425 μ m), Amoco Super A, and Alfa Aesar graphite were used. The N₂ BET surface areas of these materials were 850, 3000, and 5 m²/g, respectively. Mixtures of Amoco Super A with graphite were also densified and studied; these mixtures were 100:0, 75:25, and 50:50 Amoco: graphite on a volume basis.

In order to prevent expansion of the carbons after compaction, a special reactor was designed for use in the Cahn C1100 high pressure thermal analyzer (HPTGA). Two reactor configurations, shown in Figure 1, were used depending on whether CH₄ storage on compacted or non-compacted (loose) carbons was being measured. The sides and bottom of the cylindrical reactor were made of porous (2 μ m) stainless steel, the top of which was a solid, 3.1 mm thick disk. For loose carbons, this closing disk was placed above and supported by the hanger rod; for compacted carbons, the disk was placed over the carbon and then secured by the hanger rod, thereby preventing expansion during the HPTGA measurements. The procedures of Sosin and Quinn⁸ were used to calculate CH₄ storage capacities and pore size distributions. The densities of loose and compacted carbons were determined by knowing the weights of the carbons contained in the known reactor volume.

Densification of the Amoco carbon was studied after deposition of diethylsilane (DES). DES was chosen because it is a starting material for microporous thin films; a porous coating on the carbon would be desirable during CH₄ adsorption and desorption⁹. Two procedures were used to deposit

the DES on the carbon. In each case, two grams of Amoco carbon were treated. In one case, the carbon was soaked in 5 ml of DES for 2 hours and in the other case the carbon was soaked in a 30% solution of DES in CCl_4 for 30 minutes. Excess DES was decanted and the DES plus carbon were filtered using #1 qualitative filter paper. The carbon was subsequently air dried for 30 minutes, and then heated to 300°C in air for 15 minutes.

RESULTS

Compaction studies on two different particle size distributions, $75\text{-}38\mu\text{m}$ and $1700\text{-}425\mu\text{m}$, of the Bamebey - Sutcliffe A207 carbon were performed. Larger particles have a higher nascent density than finer particles and were anticipated to have higher compaction densities; larger particles in a loose packing situation were anticipated to have a lower density because of the voids due to irregular particle shapes. These anticipations were qualified by the data where loosely packed $75\text{-}38\mu\text{m}$ and $1700\text{-}425\mu\text{m}$ particles had densities of 0.49 and 0.44 g/ml, respectively, whereas compressed samples had maximum attainable densities of 0.82 and 0.91 g/ml, respectively. For each particle size distribution, the CH_4 storage capacity increased with increased packing density of the carbon (Figure 2). However, the highest storage capacity obtained for the A207 carbon was for the compressed $75\text{-}38\mu\text{m}$ powder even though it did not have the highest packing density.

Maximum compaction densities of only 0.34 g/ml were attainable using 100% of the Amoco carbon. It was very difficult to compact. Graphite, however, has a relatively high bulk density and is easily compacted to 1.22 g/ml. The CH_4 uptake on loose graphite is very low but compaction increases it significantly (Figure 3). In an attempt to improve the compaction properties of pure Amoco carbon, varying mixtures of carbon and graphite were prepared and subjected to CH_4 uptake determinations. Figure 4 shows the results for these blends in comparison to the pure Amoco carbon. With the 50:50 Amoco : graphite mixture, the maximum attainable density was 0.63 g/ml, almost twice that of the compacted pure Amoco carbon. The CH_4 uptake capacities increased with increased compaction densities for all blends. Interestingly, the CH_4 uptake on the compacted 75:25 Amoco : graphite mixture was the same as for 100% Amoco carbon.

The possibility of using chemical deposition on and within the pores of the Amoco carbon as a way to increase compressibility was also explored. Maximum compaction densities of 0.38 and 0.44 g/ml were attained for the high and low concentrations of DES, respectively. Even though these densities were only slightly greater than for the pure Amoco, the CH_4 uptake on the DES treated carbons was greater than on the pure carbon (Figure 5). The data suggest that DES impregnation warrants further investigation.

Pore size distributions were determined from the CH_4 isotherms. Comparison of the pore size distribution of compressed Amoco carbon relative to the loose, pure carbon indicated that compression significantly enhanced the pore volume for pores having diameters around 1.1 nm (Figure 6); pores of this dimension are believed to be optimum for CH_4 storage¹. Pore size distributions were also determined for compressed mixtures of Amoco : graphite and for the DES treated Amoco carbon (Figure 7). The total pore volume from pores with dimensions of 0.38-2.0 nm correlated well with the total CH_4 uptake (Figure 8). Plotted in Figure 8 are the average values of all replicates for the untreated and each different physically modified compressed carbon. These data also indicated similar pore volumes for the compressed, pure Amoco and for the 75:25 Amoco:graphite samples. The DES treated Amoco, especially the less severely treated material, had the highest pore volumes which was consistent with their highest CH_4 uptake capacities.

SUMMARY AND DISCUSSION

During this study, methods were explored to improve the compaction properties of porous carbons to increase the amount of CH_4 stored per unit volume of carbon. The particle size of the starting material was important and it appears that, even though larger particle can be compacted to higher densities, greater microporosity was developed during the compaction of fine powders.

Amoco Super A, a highly micro-porous carbon with low bulk density, has been shown to have a higher CH_4 uptake capacity compared to all other carbons studied during this work¹⁰. Maximum compaction densities of this carbon under the experimental conditions were low (0.34 g/ml) in comparison to graphite (1.22 g/ml). Compaction of pure graphite resulted in the development of some microporosity, which is considered responsible for uptake of 25 ml (STP) CH_4 per ml graphite. The compaction properties of a blend of graphite with the Amoco carbon were improved over those of the carbon alone and a blend of 75 : 25 carbon : graphite on a volume basis resulted

in the same amount of CH₄ adsorption as the pure carbon. These results have important implications for improving the economics of CH₄ storage on activated carbon, i.e. inexpensive graphite was substituted for the expensive activated carbon and yet the CH₄ uptake capacity was not compromised.

The role of the graphite and DES has yet to be elucidated. The data in Figure 4, where the 0.20 g/ml density sample from the 75:25 mixture has a CH₄ uptake capacity of 29 v/v, the 0.20 g/ml density sample from the 50:50 mixture has a CH₄ uptake capacity of 14 v/v and the pure Amoco carbon has a capacity of 37 v/v, suggest that in loose mixtures the effect of graphite is nearly linear in graphite concentration where it plays the role of a diluent, i.e. less Amoco carbon implies less CH₄ storage. In compressed mixtures, the diluent effect is still observant but not as predominant. Under compaction, the graphite could occupy macro-voids and provide some microporosity.

The DES coating method was chosen because of its potential to provide a porous micro-coat on and in the carbon. Quite interestingly, the data indicate that the DES treatment improved the carbon's compressibility and increased its microporosity. The DES coating did not appear to change the microporosity of non-compacted carbon.

CONCLUSIONS

The two methods for improving the compaction properties of a highly microporous carbons appear worthy of further investigation relative to fundamental and applied areas of study. Both blending carbons with a material having a higher bulk density and the chemical deposition on or within the carbon improved compaction properties and increased CH₄ uptake. Both methods appear to enhance the microporosity only after sample compaction.

REFERENCES

1. Matranga, K.R., Myers, A.L., and Glandt, E.D. *Chem. Eng. Sci.*, **47**, 1569 (1992)
2. Sheikh, M.A., Hassan, M.M., and Loughlin, K.F., *Gas Sep. Purif.*, **10**, 161 (1996)
3. MacDonald, J.A.F. and Quinn, D.F., *Carbon*, **34**, 1103 (1996)
4. MacDonald, J.A.F. and Quinn, D.F., *Fuel*, **77**, 61 (1998)
5. Alcaniz-Monge, J., De La Casa-Lillo, M.A., Cazorla-Amoros, D., and Linares-Solano, A., *Carbon*, **35**, 291 (1997)
6. Wojtowicz, M.A., Smith, W.W., Serio, M.A., Simons, G.A., and Fuller, W.D., Extended Abstracts, 23rd Biennial Conference on Carbon, Univ. Park, PA, USA, 342, 1997
7. Stewart, M.L. and Stencel, J.M., *Preprints Symposium on Alternate Uses for Fossil Fuels*, ACS, Division of Fuel Chem., Denver, CO Meeting, 408, March., 1993
8. Sosin, K.A. and Quinn, D.F., *J. Porous Materials*, **1**, 111 (1995)
9. Levy, R.A., Ramos, E.S., Krasnoperov, L.N., Datta, A., and Grow, J.M., *J. Mater. Res.*, **11**, 3164 (1996)
10. Stencel, J.M., Ban, H., Li, T.-X., Neathery, J.K., Rubel, A.M., and Schaefer, J.L., Annual Report, NASA/EPSCoR, Materials Processing for Space Mission Energy Needs, April 1, 1996 - March 31, 1997

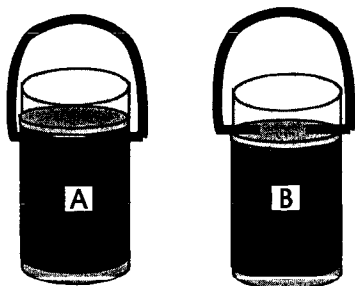


Figure 1. Reactor configurations for CH₄ storage determinations on loose (A) and compressed (B) carbons.

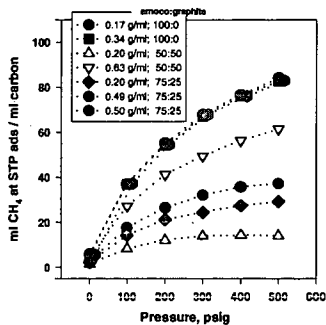


Figure 4. CH₄ storage on loose and compressed mixtures of Amoco Super A and graphite.

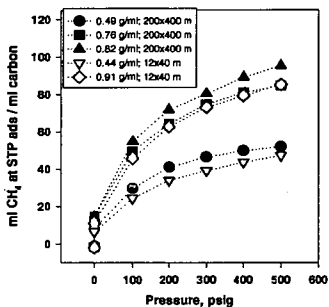


Figure 2. CH₄ storage on loose and compressed 75-38µm and 1700-425µm particle fractions of an activated carbon.

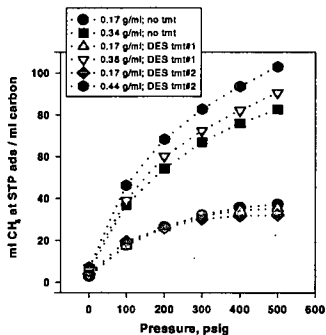


Figure 5. CH₄ storage on loose and compressed untreated and DES treated Amoco Super A carbon.

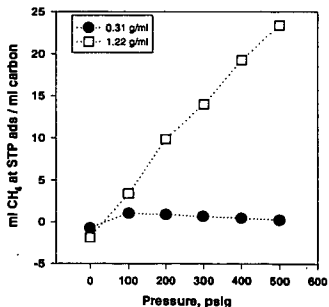


Figure 3. CH₄ storage on loose and compressed graphite.

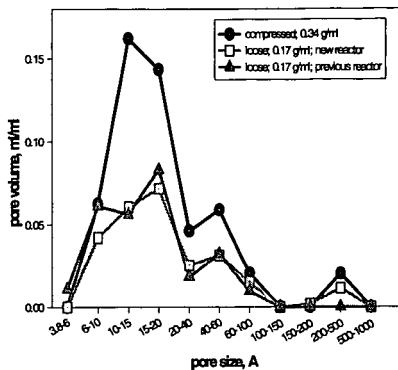


Figure 6. Pore size distributions for loose and compressed Amoco Super A carbon.

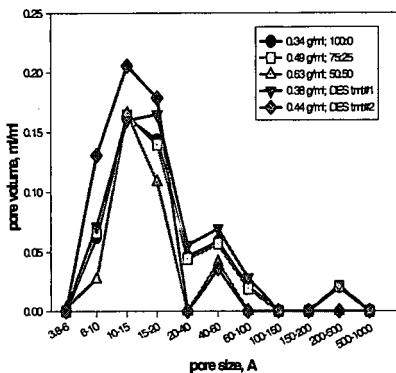


Figure 7. Comparison of the pore size distributions of compressed untreated carbon, carbon-graphite mixtures, and DES treated carbons.

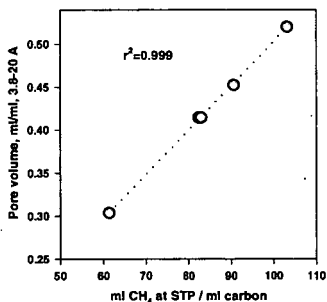


Figure 8. Correlation of pore volume of 3.8-20 Å pores with CH₄ storage capacity.

PREDICTING CH₄ ADSORPTION CAPACITY OF MICROPOROUS CARBON USING N₂ ISOTHERM AND A NEW ANALYTICAL MODEL

Jian Sun,¹ Scott Chen,² Massoud Rostam-Abadi^{1,2} and Mark J. Rood,*¹

¹ Department of Civil and Environmental Engineering, University of Illinois at Urbana-Champaign (UIUC), 205 North Mathews Avenue, Urbana IL 61801, USA

² Illinois State Geological Survey (ISGS), 615 East Peabody Drive, Champaign IL 62810, USA

ABSTRACT

A new analytical pore size distribution (PSD) model was developed to predict CH₄ adsorption (storage) capacity of microporous adsorbent carbon. The model is based on a 3-D adsorption isotherm equation, derived from statistical mechanical principles. Least squares error minimization is used to solve the PSD without any pre-assumed distribution function. In comparison with several well-accepted analytical methods from the literature, this 3-D model offers relatively realistic PSD description for select reference materials, including activated carbon fibers. N₂ and CH₄ adsorption data were correlated using the 3-D model for commercial carbons BPL and AX-21. Predicted CH₄ adsorption isotherms, based on N₂ adsorption at 77 K, were in reasonable agreement with the experimental CH₄ isotherms. Modeling results indicate that not all the pores contribute the same percentage V_m/V_s for CH₄ storage due to different adsorbed CH₄ densities. Pores near 8-9 Å shows higher V_m/V_s on the equivalent volume basis than does larger pores.

INTRODUCTION

Activated carbon usually has a heterogeneous pore structure due to the structural complexity and randomness.¹ The distribution of pore sizes is a critical parameter for characterizing the adsorbent, when the adsorption potential is a dominant factor. Adsorption density is strongly dependent on the adsorbent's pore size (w). For instance, adsorption is enhanced in micropores ($w < 20$ Å) due to overlap of the force field created by the opposing pore walls. For applications such as natural gas storage, the adsorbent should be prepared in such a way that it has minimum mesopore (20 Å $< w < 500$ Å) and macropore ($w > 500$ Å) volume and maximum micropore volume. In particular, w for micropores should be near 8 Å; the optimal pore size for CH₄ adsorption.² In this study w is defined as the distance between the edges of the carbon atoms in opposite pore walls. The pores are modeled as slits consisting of two infinite graphite planes.

A number of PSD models have been developed on the basis of N₂ adsorption at 77 K. Although the models provide great insights, there is apparent lack of consistency in the modeled PSD results³ due to their different theoretical foundations and assumptions. Well-accepted PSD characterization methods include MP,⁴ DRS,⁵ JC,⁶ HK⁷ and, more recently, SNAP^{8,9} and DFT.¹⁰ SNAP is one of the latest PSD methods based on numerical results from Mean-Field Density Functional Theory (MFT).^{8,9} SNAP uses a pre-assumed log normal distribution function to model N₂ adsorption at 77 K. DFT (Micromeritics) is one of the latest PSD methods based on Non-local MFT.¹⁰ DFT employs a Regularization technique to solve the generalized adsorption isotherm (GAI)^{8,11} which results in a discrete PSD. Another version of DFT (Quantachrome) is based on Local MFT, which neglects the adsorbate-adsorbate interactions.

The objective of this study is to model and correlate N₂ and CH₄ adsorption on microporous carbon through an analytical approach. A PSD model is developed on the basis of a 3-D isotherm equation without pre-assumed distribution functions. Prediction of CH₄ adsorption isotherm is carried out by correlating the N₂ and CH₄ adsorption for select adsorbents.

MODEL DESCRIPTION

Taking an approach similar to Chen and Yang's 2-D adsorption isotherm equation,¹² a 3-D adsorption isotherm equation was developed,¹³

$$\ln \frac{\rho^s}{\rho^g} + \frac{8\eta - 9\eta^2 + 3\eta^3}{(1-\eta)^3} + \frac{1}{k_b T} \frac{a}{b} \left(\ln(1+4\eta) - \frac{4\eta}{1+4\eta} \right) + \frac{\Phi}{k_b T} = 0 \quad (1)$$

for a given pore size and geometry (slits), with a mean force field Φ . The classical Dubinin-Stoeckli (DS) inverse relationship,¹⁴ is used for its simplicity to evaluate the mean force field as a function of pore size. ρ^g and ρ^s are volume number densities of the gas and adsorbed phases,

respectively. η is the pore filling fraction. The second term in Eq. 1 describes the short-range repulsive force between adsorbate molecules, while the third term represents the long-range attractive force between adsorbate molecules. The fourth term refers to the interaction between adsorbate and adsorbent. For low adsorption density (close to bulk gas density), the packing fraction is close to zero (so are the second and third terms in Eq. 1), thus the equation reduces to Henry's law. In comparison with the 2-D equation,¹² 3-D adsorption density can be obtained with the 3-D equation. Therefore, N_2 and CH_4 adsorption density and PSD based on N_2 adsorption can be determined.

For N_2 adsorption at 77 K, phase transition from gas to liquid takes place in micropores when adsorption density increases substantially due to pore filling. To include this feature and assure a realistic adsorption density, a modified DR equation is used to calculate adsorption density after pore filling,¹⁵

$$\rho = \rho_l \exp \left[- \left(\frac{A}{\beta E_0} \right)^2 \right] \quad (2)$$

where ρ is the density of adsorbed phase. ρ_l is the density of saturated liquid N_2 . A is the differential molar work, β is the affinity coefficient and E_0 is the adsorption characteristic energy. The pore filling fraction θ can be expressed as ρ/ρ_l .

Correlation between pore filling pressure and critical pore size in the 3-D model was obtained from MFT^{8,9} to describe the discontinuous jump in the N_2 adsorption isotherm.¹³ In other words, the adsorption densities prior to and after pore filling are calculated by the 3-D equation and by the modified DR equation, respectively.

To obtain the PSD, the GAI is formulated as:^{8,11}

$$n(P^r) = \int_0^{\infty} \rho(P^r, w) f(w) dw \quad (3)$$

$n(P^r)$ is the amount of adsorbed N_2 at a relative pressure $P^r (= P/P_0)$ obtained directly from the experimental adsorption isotherm, $\rho(P^r, w)$ is the adsorbate density calculated using the 3-D adsorption isotherm (Eq. 1) and modified DR equation (Eq. 2), and $f(w)$ is the distribution of pore volume as a function of w . Eq. 3 is broken down into a set of linear equations solved using least squares error minimization.¹³

MATERIALS USED

Two activated carbon fiber (ACF) samples (ACF-15 and ACF-25) obtained from American Kynol, Inc. (New York, NY) were used as adsorbents for PSD modeling. ACF-15 has the shorter activation time (lower burn-off and higher yield) compared to ACF-25. Norit Row (American Norit) is used to compare PSD results by DFT and the 3-D model. N_2 adsorption data and DFT results for Norit Row were obtained from Kruk.¹⁶ Other commercial carbons used are BPL (Calgon Carbon), and AX-21 (Amoco). The 77 K N_2 adsorption isotherm of BPL and AX-21 was measured with a Micromeritics ASAP2400 (P/P_0 : 10^{-3} to 1).

RESULTS AND DISCUSSION

Optimal Pore Size for CH_4 Adsorption

Multiple layer adsorption does not occur at ambient temperature for CH_4 because it is a supercritical gas. Therefore, there must be an optimal pore size associated with the maximum CH_4 adsorption density. Densities of adsorbed CH_4 at 3.4 MPa (500 psia) and 300 K on an ideal adsorbent with various pore sizes are calculated using Eq. 1. The affinity coefficient β for CH_4 is calculated using the following equation

$$\beta = \frac{[P^r]}{[P^r]_0} = 0.353 \quad (4)$$

$[P^r]$ and $[P^r]_0$ are the parachors of CH_4 and benzene, respectively, which can be obtained from standard references.¹⁷ Dependence of adsorbed CH_4 density on pore size is plotted in Figure 1. The optimal pore size with a maximum adsorption capacity is $\approx 8.0 \text{ \AA}$, closely matching the results obtained by computer simulation.²

PSD Characterization of Activated Carbon Fibers

PSDs for ACF-15 and ACF-25 obtained by the 3-D model are presented in Figure 2. The

micropore volume and pore volume for $w < 100 \text{ \AA}$ from the 3-D model are 0.363 and 0.988 cm^3/g respectively (Table 1). Increased pore volume and pore widening are expected for ACF-25 compared to ACF-15. These features are well illustrated in Figure 2. Calculated N_2 isotherms using the 3-D model and the corresponding experimental isotherms for the two ACF samples are also presented in Figure 2. Good agreement exists in all cases.

Comparisons of PSD results for ACF-25 by MP, JC, HK and the 3-D model are summarized in Figure 3. In contrast to the PSDs by JC and HK, a multiple modal PSD for ACF-25 is revealed by the 3-D model, which corresponds to the inflections in the experimental isotherm. MP method indicates the PSD maximum is about 8 \AA (Table 1). This is due to the MP method not considering the enhanced adsorption in micropores. The adsorption film thickness (related directly to estimated pore size in the MP method) should be greater in micropores than for non-porous materials at a given relative pressure. MP method tends to underestimate the pore size for micropores. The PSD obtained by JC method predicts a single mode and extends further into the mesopore region (maximum at 16 \AA). Such result is presumably caused by use of the DR equation and the initial constraint associated with the pre-assumed normal distribution for the PSD. Compared with the others, HK method gives the smallest PSD maxima for both ACF samples (Table 1). It does not appear to respond well to pore widening brought about by the extent of activation for ACF-25. HK method underestimates the pore size due to the progressive pore filling mechanism.

Comparison of PSDs by DFT and 3-D Model

PSD results using the DFT method¹⁰ for Norit Row is provided in Figure 4. The PSD results by DFT are reproduced by normalizing the pore volumes to the corresponding pore size intervals and taking the center point of each size interval as the corresponding pore size. PSD by DFT is usually presented as a discrete bar chart.^{18,19} PSD results by the 3-D model based on the same N_2 isotherm is also plotted in Figure 4. Reasonable agreement can be observed between the two methods, although the PSD maximum by DFT is 0.5 \AA larger than that by the 3-D model.

Prediction of CH_4 Adsorption Isotherm

Prediction of CH_4 adsorption isotherm at 296 K is carried out with BPL and AX-21 (Figure 5), whose experimental CH_4 adsorption isotherms were obtained from Sosin.²⁰ The 3-D equation is used to calculate the CH_4 adsorption densities (with volume exclusion but no pore filling because CH_4 is supercritical), which are then combined with the modeled PSDs to obtain CH_4 adsorption isotherms at 296 K. It is noticed that CH_4 adsorption is overestimated in the low pressure region and underestimated in the high pressure region by the 3-D model. This is possibly due to the use of the DS inverse relationship to calculate the adsorption potential energy for CH_4 adsorption. In comparison with experimental results based on a molecular probe study,²¹ the DS inverse relationship overestimates the adsorption potential. The potential by the DS relationship also decreases rapidly as the pore size increases,²² resulting in underestimated adsorbed CH_4 density. Using the DS relationship for N_2 adsorption cannot offset this effect, since the modified DR equation is used to calculate the adsorption density after complete pore filling. At high adsorptive pressures, the adsorption density is close to the value of liquid N_2 , when the DS relationship has negligible contribution to the adsorption density. The prediction may be improved by using other more sophisticated yet more complicated correlation like the HK relationship for carbon and CH_4 .

Modeling results indicate that not all the pores contribute the same percentage Vm/Vs for gas storage due to different adsorbed CH_4 densities. Micropores near 8-9 \AA shows greater volumetric CH_4 capacity (Vm/Vs) on the equivalent volume basis than does larger pores. Figures 6 and 7 plot the percentage of pore volume and percentage of Vm/Vs contributed by the pores of ~8, ~9 and ~20 \AA as functions of activation weight loss for a coal-based carbon series.²³ Around 75% weight loss, volume of ~8 \AA pores represents only 22% of the total pore volume (percentage pore volume = 22%), but contribute 39% of the total adsorbent's Vm/Vs . The ratio of percentage Vm/Vs to percentage pore volume is 1.8 for ~8 \AA pores. Similar results can be observed for ~9 \AA pores. The ratio of % Vm/Vs to % pore volume is 1.6 for ~20 \AA pores. The ratio is reduced for mesopores and macropores due to the sharp decrease of adsorbed CH_4 density in these pores.

SUMMARY AND CONCLUSIONS

A new analytical PSD model has been developed by solving the GAI for N_2 adsorption at 77 K using least squares error minimization. Local isotherms for each single pore size is calculated

using a 3-D adsorption isotherm equation, derived from statistical mechanical principles. In comparison to select analytical methods from the literature, this 3-D model offers a relatively realistic PSD description for select reference materials. N₂ and CH₄ adsorption is correlated using the 3-D model for BPL and AX-21. Predicted CH₄ adsorption isotherms are in reasonable agreement with experimental CH₄ isotherms.

Acknowledgments. AX-21 was provided by Mega-Carbon Co. N₂ isotherms for ACFs and Norit Row were provided by Drs. Mark Cal and Anthony Lizzio of ISGS and Drs. Michal Kruk and Mietek Jaroniec of Kent State University.

REFERENCES

1. Gregg, S.J. and Sing, K.S.W. *Adsorption, surface area and porosity* Academic, London, 1984
2. Matranga, K.R.; Stella, A.; Myers, A.L.; Glandt, E. D. *Chem. Eng. Sci.* **1992**, *47*, 1569.
3. Russell, B.P.; LeVan, M.D. *Carbon* **1994**, *32*, 845.
4. Mikhail, R.Sh.; Brunauer, S.; Bodor, E.E. *J. Colloid Interface Sci.* **1968** *26* 45
5. Stoeckli, H.F. *J. Colloid Interface Sci.* **1977**, *59*, 184.
6. Jaroniec, M.; Choma, J. *Mater. Chem. Phys.* **1986**, *15*, 521.
7. Horvath, G.; Kawazoe, K. *J. Chem. Eng. Jpn.* **1983**, *16*, 470.
8. Seaton, N.A.; Walton, J.P.R.B.; Quirke, N. *Carbon* **1989**, *27*, 853.
9. Lastoskie, C.; Gubbins, K.E.; Quirke, N. *J. Phys. Chem.* **1993**, *97*, 4786.
10. Olivier, J.P. *J. Porous Mater.* **1995**, *2*, 9.
11. McEnaney, B. *Carbon* **1988**, *26*, 267.
12. Chen, S.G.; Yang, R.T. *Langmuir* **1994**, *10*, 4244.
13. Sun, J.; Rood, M.J.; Rostam-Abadi, M. in *Extended Abstract the 23rd Biennial Conference on Carbon*, State College, PA, 1997, pp. 348
14. Dubinin, M.M. in *Progress in Surface and Membrane Science* Academic 1-70, 1975
15. Sun, J.; Brady, T.A.; Rood, M.J.; Lehmann, C.M.; Rostam-Abadi, M.; Lizzio, A.A. *Energy and Fuel* **1997**, *11*, 316. (b)
16. Kruk, M.; Jaroniec, M. *Adsorption* **1996**, *3*, 209.
17. Quayle, O.R. *Chem. Rev.* **1953**, *53*, 439.
18. Kruk, M.; Jaroniec, M. in *Extended Abstract the 23rd Biennial Conference on Carbon*, State College, PA, 1997, pp. 106
19. Olivier, J.P.; Conkin, W.B.; Szombathely, M.V. in *Characterization of Porous Solids III* Elsevier Amsterdam, 1994
20. Sosin, K.A.; Quinn, D.F. *J. Porous Material* **1995**, *1*, 111.
21. McEnaney, B. *Carbon* **1987**, *25*, 457.
22. Chen, S.G.; Yang, R.T. *J. Colloid Interface Sci.* **1996**, *177*, 298.

Table 1 Summary of PSD information for ACFs-15 and 25 by MP, JC, HK and the 3-D Model

Method	ACF-15			ACF-25		
	PSD Max. [Å]	Micropore volume [cm ³ /g]	Pore volume [cm ³ /g]	PSD Max. [Å]	Micropore volume [cm ³ /g]	Pore volume [cm ³ /g]
MP	5.1	0.318	0.322	7.7	1.066	1.109
JC	9.5	0.343	0.343	15.5	0.504	0.865
HK	5.3*	0.333	0.336	5.8	0.801	0.843
3-D	7.0	0.363	0.363	9.0	0.988	1.070

* Actual maximum should be less.

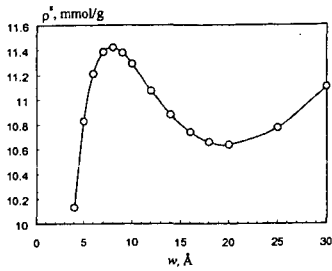


Figure 1 The optimal pore size for CH₄ adsorption.

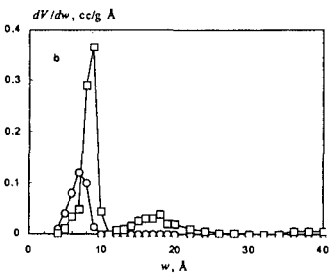
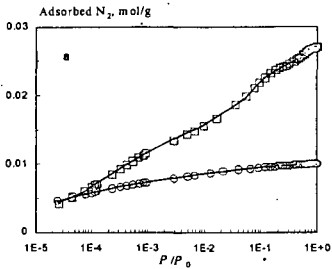


Figure 2 Experimental (symbols) and calculated (lines) N₂ adsorption isotherm at 77 K (a) and PSDs for ACF-15 (circles) and 25 (squares) by the 3-D model (b).

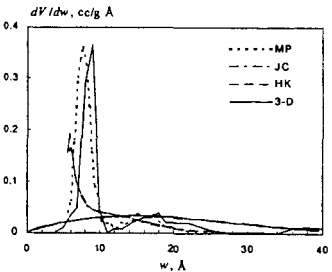


Figure 3 Comparison of PSDs for ACF-25 by MP, JC, HK and the 3-D model.

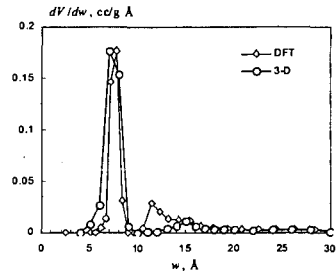


Figure 4 PSD results for Norit Row by DFT and the 3-D model.

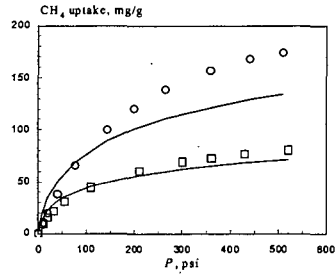


Figure 5 Experimental (symbols) and predicted (lines) CH₄ adsorption isotherms for AX-21 (circles) and BPL (squares).

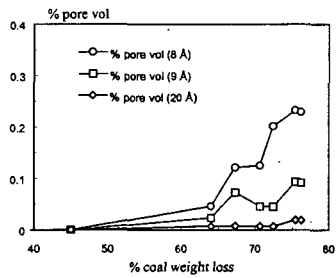


Figure 6 Percentage pore volume vs weight loss in the preparation of a serial coal-based steam-activated carbon at 800°C.

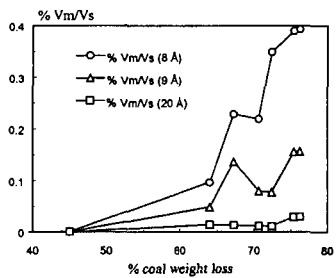


Figure 7 Percentage Vm/Vs vs weight loss.

MULTICOMPONENT DISCHARGE DYNAMICS OF ADSORBED NATURAL GAS STORAGE SYSTEMS

José P. B. Mota

Departamento de Química, Faculdade de Ciências e Tecnologia, Universidade Nova de Lisboa,
2825 Monte de Caparica, Portugal

ABSTRACT

Adsorption storage on highly microporous activated carbon is the most promising low-pressure alternative for storing natural gas. A detailed mathematical model has been developed in order to study the impact of natural gas composition on cycling efficiency of adsorption storage systems. Results show that net deliverable capacity is substantially decreased by heavy hydrocarbons which are present in small amounts in natural gas. Economical means of removing them from the gas stream before charge need to be identified and evaluated.

INTRODUCTION

Natural gas (NG) has always been considered a potentially attractive fuel for vehicle use. It is cheaper than gasoline and diesel, the technical feasibility of NG vehicles is well established, and they have a less adverse effect on the environment than liquid-fueled vehicles. For example, NG can be burnt in such a way as to easily minimize NO_x and CO emissions [1]. In fact, NG outperforms petroleum based fuels in every aspect except on-board storage [2].

A large effort has been devoted to replacing NG high-pressure compression by an alternative storage method working at pressures up to 3.5 MPa. Besides allowing the use of lighter and safer on-board storage reservoirs, this upper pressure limit is easily achieved with a single-stage compressor or, alternatively, the vehicle can be refueled directly from a high-pressure pipeline. As a result, a significant decrease in the capital and operating costs of refuelling stations would be obtained.

A general consensus has been reached regarding adsorption as the most promising low-pressure alternative for storing NG. Extensive experimental work has shown that highly microporous activated carbon is the adsorbent best suited for his task. Quinn and co-workers [1] have given a detailed review of the subject and an update will be published soon [3].

Several operational problems that influence the success of adsorbed natural gas (ANG) storage have been addressed in the literature [1,2]. The one of concern here is the storage capacity loss due to the gradual contamination of the adsorbent with hydrocarbons higher than methane, which are present in trace amounts in NG. If these are not removed from the gas stream before charge, they can adsorb preferentially to high equilibrium residual levels and substantially decrease the net deliverable capacity. This is a consequence of their higher adsorption potential and of the infeasibility of operating an on-board storage reservoir at sub-atmospheric pressures.

Although some work, both analytical and experimental, has been conducted to design and test economical means of controlling the contaminants [4], very little effort has been devoted to the study of their impact on cycling efficiency. This has prompted the author to conduct the work presented here.

PROBLEM FORMULATION

In order to assess the impact of NG composition on net deliverable capacity, the dynamic behaviour of an on-board storage cylinder is modeled as a series of consecutive cycles, each consisting on charge with a fixed gas mixture followed by discharge at constant molar rate until depletion pressure is reached.

Gas adsorption.

Multicomponent adsorption equilibrium is predicted by a formalism combining Adsorption Potential [5] and Ideal Adsorbed Solution (IAS) [6] theories. The same idea has been applied by Stoekli *et al.* [7] to the binary adsorption of vapours using the Dubinin-Radushkevich isotherm.

Recently, Chang and Talu [8] studied theoretically and experimentally the performance of adsorbed methane storage cylinders under discharge conditions. Their experimental adsorption isotherms are shown in figure 1a. The analysis of these data on the basis of the potential theory results in a characteristic curve of adsorption on the carbon which is depicted in figure 1b. The constructed curve is temperature-independent, this fact corroborates the applicability of the theory. Saturation pressure and adsorbed molar volume, V_A , were calculated according to expressions proposed by Ozawa *et al.* [9].

In many cases, the theory can be generalized if an affinity coefficient, β , is used as shifting factor to bring the characteristic curves of all gases on the same adsorbent into a single curve. This is assumed to apply to all the species under consideration here. Based on the author's past

experience on light hydrocarbon adsorption, the liquid molar volume of the adsorbate at the normal boiling point was used as the affinity coefficient.

Although the functional form of the characteristic curve is adsorbent dependent, expressing the logarithm of the adsorbed phase volume, W , as a truncated series development of the scaled adsorption potential, ϵ/β , provides good fitting of the experimental data [9]. A second-order polynomial is usually enough, as can be seen in figure 1b.

Multicomponent adsorption equilibrium prediction using the IAS method requires values of spreading pressure, Π , for adsorption of single gases. According to the potential theory, if this variable is scaled by V_A/β then it becomes a function of ϵ/β only, and can be computed from a single curve for all intervening adsorbates:

$$A\Pi_i^* \equiv (V_A/\beta)_i A\Pi_i = \int_{\epsilon_i/\beta_i}^{\infty} W(\epsilon^*) d\epsilon^* \quad (i = 1, \dots, N). \quad (1)$$

If the development of $\ln W$ as a power series of ϵ/β accurately describes the experimental data, then eq. (1) suggests that $A\Pi^*$ can also be expressed as a series development of the form

$$\ln(A\Pi_i^*/A\Pi_0^*) = \sum_{n=1}^{n=\infty} k_n (\epsilon_i/\beta_i)^n, \quad k_1 < 0, \quad (2)$$

where $A\Pi_0^*$ is the value of $A\Pi^*$ at saturation. As shown in figure 2a, a truncated second-order polynomial expansion describes very accurately the experimental data under consideration. Furthermore, the truncated series is easily invertible,

$$\epsilon_i/\beta_i = \frac{k_1}{2k_2} \left[\sqrt{1 + (4k_2/k_1^2) \ln(A\Pi_i^*/A\Pi_0^*)} - 1 \right], \quad (3)$$

which is critical in speeding up the computations.

Discharge phase.

The model employed for the discharge phase is an extension to multicomponent adsorption of a prior model [10,11] that has been proven experimentally to describe successfully the discharge dynamics of methane adsorptive storage cylinders [8].

In an on-board storage reservoir the discharge rate is controlled by vehicle power requirements. This process is slow enough for pressure to be uniform within the cylinder and for the inexistence of intraparticle gradients. Hence, an equilibrium model can be employed at the particle level. Moreover, the cylinder is considered sufficiently long so that the small axial temperature gradient induced by the front and rear faces has negligible impact on the overall dynamics. These assumptions drastically reduce the spatial dimensionality of the problem, since only the radial profile needs to be taken into account. The implication of these assumptions on model performance is discussed to further length elsewhere [10].

The differential material balance for component i on a cylindrical shell element of the reservoir located at radial position r , can be written as

$$\epsilon \frac{\partial c_i}{\partial t} + \rho_b \frac{\partial q_i}{\partial t} - \frac{\epsilon}{r} \frac{\partial}{\partial r} \left(r D_{e,i} c \frac{\partial y_i}{\partial r} \right) + y_i F = 0 \quad (i = 1, \dots, N), \quad (4)$$

where c_i and q_i are the concentrations in gas and adsorbed phase, respectively, y_i is the mole fraction in gas, ϵ and ρ_b are the porosity and bulk density of the carbon bed, and $F(t, r)$ is the local contribution to the overall molar discharge rate per unit reservoir volume.

These balances are subjected to boundary conditions

$$\partial y_i / \partial r = 0 \quad \text{for } r = 0, R_0 \quad (i = 1, \dots, N), \quad (5)$$

where R_0 is the cylinder radius.

As discharge proceeds, the consumed heat of adsorption is only partially compensated by the wall thermal capacity and by the heat transferred from the outside air. As a result, a radial temperature profile develops in the medium, the major temperature drop occurring at the centre of the bed. Given that pressure remains uniform within the cylinder, the temperature profile induces radial concentration gradients in both adsorbed and gas phases. The latter tend to be lessened by bulk diffusion which is taken into account in the third term of eq. (4).

Accordingly, the local contribution F must also vary along r in order to ensure uniform pressure in the cylinder and to satisfy the following integral constraint over the cross section of the cylinder:

$$2\pi L \int_0^{R_0} F(t, r) r dr = Q, \quad (6)$$

where L is the cylinder length and Q is the imposed overall molar discharge rate.

The energy equation, applied to the same differential volume, yields

$$\left[\rho_b C_s + C_g (\varepsilon c + \rho_b q) \right] \frac{\partial T}{\partial t} - \varepsilon \frac{dP}{dt} + \rho_b \sum_i (-\Delta H)_i \frac{\partial q_i}{\partial t} - \frac{1}{r} \frac{\partial}{\partial r} \left(r \lambda_e \frac{\partial T}{\partial r} \right) = 0, \quad (7)$$

where C_s and C_g are the carbon and gas heat capacities, respectively, T is temperature, P is gas pressure, $-\Delta H_i$ is the heat of adsorption for species i , and λ_e is the effective thermal conductivity of the carbon bed.

Equation (7) is subjected to boundary conditions

$$\partial T / \partial r = 0 \quad \text{for } r = 0, \quad (8)$$

$$\left(1 + \frac{e_w}{2R_o} \right) e_w C_w \frac{\partial T}{\partial t} + \lambda_e \frac{\partial T}{\partial r} = \left(1 + \frac{e_w}{R_o} \right) h_w (T_{\text{amb}} - T) \quad \text{for } r = R_o. \quad (9)$$

The latter condition is an energy balance on the steel cylinder wall, it cannot be neglected due to its large thermal capacity. Symbols e_w , C_w and h_w represent wall properties (thickness, volumetric heat capacity, and natural convection heat transfer coefficient at the external surface, respectively) and T_{amb} is ambient temperature.

Charge phase.

Heat effects during the charge phase are neglected mainly because adequate solutions have been proposed to eliminate them. For example, at a refuelling station the gas can be cooled before charging the reservoir or an external NG recycle loop can remove the heat and reject it to the environment across an air-cooled heat exchanger [12]. Alternatively, fleet vehicles can be charged over a long period, e.g. overnight, which provides enough time to dissipate the heat of adsorption. The interested reader is referred to Mota [10] for rigorous modeling work on heat effects in the fast charge of ANG storage cylinders.

According to these assumptions, a lumped-based model can be adopted for the charge phase. At the end of the discharge, the residual amount of each component left in storage per unit reservoir volume is computed from

$$S_i = (2/R_o) \int_0^{R_o} (\varepsilon c_i + \rho_b q_i) r dr \quad \text{at depletion} \quad (i = 1, \dots, N). \quad (10)$$

Then, the following set of lumped material balances is solved in order to compute the new discharge initial conditions:

$$\varepsilon c_i + \rho_b q_i = S_i + z_i F_c \quad \text{with } P = P_{\text{charge}} \quad \text{and } T = T_{\text{amb}} \quad (i = 1, \dots, N), \quad (11)$$

where F_c is the amount of gas admitted to the cylinder during charge and z_i is its mole fraction composition. F_c is an unknown which is computed along with the new initial discharge conditions.

RESULTS AND DISCUSSION

Unfortunately, due to lack of space most of the paper has been spent describing the theoretical model, leaving room for a limited amount of results. The discharge phase model is validated for single-gas adsorption by comparison with the experimental temperature history in an adsorbed methane cylinder during discharge. As shown in figure 2b, model results are in close agreement with the experimental data.

Multicomponent discharge dynamics is summarized in figures 3a and 3b. It is a complex function of the adsorption potential of each component and its mole fraction in the charge gas. Depletion pressure is 1.4 atm while charge pressure is 35 atm. The discharge flow rate considered, 6.7 l/min, produces a methane discharge duration of about 4 hours under non-isothermal conditions. Table 1 lists the values of the main parameters employed in the numerical simulations. The gas composition considered in this study is given in table 2, it characterizes the NG from the Hassi R'Mel well supplying Portugal.

The net deliverable capacity is measured in terms of dynamic efficiency, which for component i is defined as

$$\eta_i = \frac{\text{amount of species } i \text{ delivered under dynamic conditions}}{(\text{amount of pure methane delivered isothermally}) \cdot z_i}, \quad (12)$$

where z_i is its mole fraction in the charge gas (table 2). This way, the η values converge to a common point at the cyclic steady state (figure 3a). The dynamic efficiency decreases gradually with the number of cycles to the cyclic steady-state value, although it attains a maximum at intermediate cycles for the higher hydrocarbons if their mole fractions in the charge gas are high enough. Until steadiness is reached, the total hydrocarbon capacity loss (C_1-C_5) depends linearly on the logarithm of the number of cycles. This is agreement with the experimental observations of Golovoy and Blais [13] for 100 cycles of operation of an ANG cylinder.

The temperature and mole fractions shown in figure 3b are lumped values obtained from averaging the variable over the cross section of the cylinder. The same figure shows that the discharge duration is reduced as the number of cycles is increased since the micropore volume is gradually occupied by the higher hydrocarbons which tend to remain adsorbed at depletion pressure. The temperature history is approximately linear, because the discharge is carried out at constant molar rate, and is nearly insensitive to the cycle number.

CONCLUSIONS

A detailed mathematical model has been developed in order to study the impact of NG composition on cycling efficiency of ANG reservoirs. Although the model has been applied to a single NG, other gas compositions should produce the same qualitative behaviour. The results emphasize the need to identify and evaluate economical means of removing the contaminants from the gas stream before charge. The solution could be either a gas clean-up system installed at the refueling station [4,12] or a guard bed placed in front of the on-board storage reservoir [14].

ACKNOWLEDGEMENTS

Financial support received from PRAXIS XXI (PCEX/C/QUI/109/96) and from FLAD is gratefully acknowledged.

REFERENCES

1. N. D. Parkyn and D. F. Quinn, In *Porosity in Carbons* (Edited by J. Patrick), pp. 291–325. Edward Arnold, London (1995).
2. O. Talu, Proceedings 4th International Conference on Fundamentals of Adsorption, Kyoto, Japan, pp. 655–662 (1993).
3. T. L. Cook, C. Komodromos, D. F. Quinn and S. Ragan, In *Carbon Materials for Advanced Technologies* (Edited by T. Burchell). Elsevier, in press.
4. M. Sejnoha, R. Chahine, W. Yaïci, and T. K. Bose, Paper presented at AIChE Meeting, San Francisco (1994).
5. S. Brunauer, *The adsorption of gases and vapours*. Oxford University Press, Princeton (1945).
6. A. L. Myers and J. M. Prausnitz, *AIChE J.* **11**, 121–127 (1965).
7. F. Stoeckli, D. Wintgens, A. Lavanchy, and M. Stöckli, *Adsorp. Sci. Technol.* **15**, 677–683 (1997).
8. K. J. Chang and O. Talu, *Appl. Thermal Engng* **16**, 359–374 (1996).
9. S. Ozawa, S. Kusumi, and Y. Ogino, *J. Coll. Int. Sci.* **56**, 83–91 (1976).
10. J. P. B. Mota, *Modélisation des transferts couplés en milieux poreux*, Ph.D. Thesis, Institut National Polytechnique de Lorraine, France (1995).
11. J. P. B. Mota, A. E. Rodrigues, E. Saadjan, and D. Tondeur, *Carbon* **35**, 1259–1270 (1997).
12. W. E. BeVier, J. T. Mullhaupt, F. Notaro, I. C. Lewis, and R. E. Coleman, Paper presented at 1989 SAE Future Transportation Technology Conference and Exposition, Vancouver (1989).
13. A. Golovoy and E. J. Blais, In *Alternate Fuels for Special Ignition Engines*, p. 47. SP-559 SAE Conference Proceedings, Warrendale, PA 15096 (1983).
14. T. L. Cook, C. Komodromos, D. F. Quinn, and S. Ragan, Paper presented at Windsor Workshop on Alternative Fuels, Toronto (1996).

$C_g = 355.5 \text{ atm}\cdot\text{cm}^3\cdot\text{mol}^{-1}\cdot\text{K}^{-1}$	$P_{\text{depletion}} = 1.4 \text{ atm}$
$C_s = 10.38 \text{ atm}\cdot\text{cm}^3\cdot\text{g}^{-1}\cdot\text{K}^{-1}$	$R_o = 10 \text{ cm}$
$C_w = 38.68 \text{ atm}\cdot\text{K}^{-1}$	$T_{\text{amb}} = 20 \text{ }^\circ\text{C}$
$e_w = 0.55 \text{ cm}$	$\varepsilon = 0.5$
$L = 74 \text{ cm}$	$\lambda_e = 1.26 \text{ atm}\cdot\text{cm}^2\cdot\text{min}^{-1}\cdot\text{K}^{-1}$
$P_{\text{charge}} = 35 \text{ atm}$	$\rho_b = 0.481 \text{ g}\cdot\text{cm}^{-3}$

Table 1: Data employed in numerical simulations.

Component	CH ₄	C ₂ H ₆	C ₃ H ₈	C ₄ H ₁₀	C ₅ H ₁₂	N ₂
Mole fraction	0.840	0.076	0.020	0.007	0.003	0.054

Table 2: Composition of natural gas from the Hassi R'Mel well (Algeria) supplying Portugal.

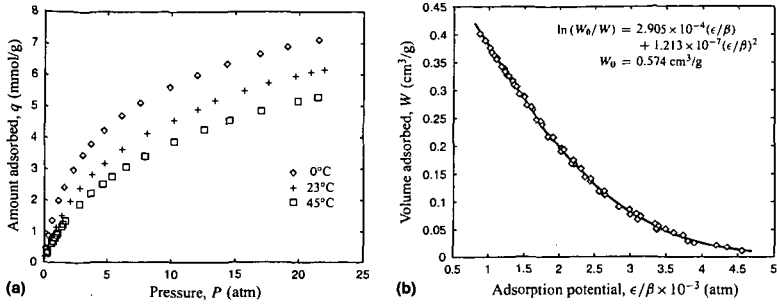


Figure 1: Methane adsorption on an activated carbon. (a) Experimental isotherms reported by Chang and Talu [8]; (b) corresponding characteristic curve of adsorption plotted according to the potential theory.

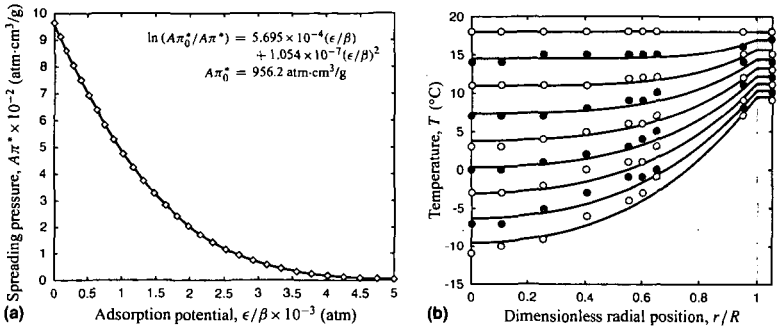


Figure 2: (a) Spreading pressure as a function of scaled adsorption potential for the carbon under study. (b) Radial temperature profiles in an adsorbed methane cylinder as a function of time during discharge. Comparison between experiments [8] (points) and model predictions (lines). Sampling interval = 20 min; $L = 74$ cm, $R = 10$ cm, carbon weight = 15.78 kg, discharge rate = 6.7 l/min, charge pressure = 21 atm, depletion pressure = 1.6 atm.

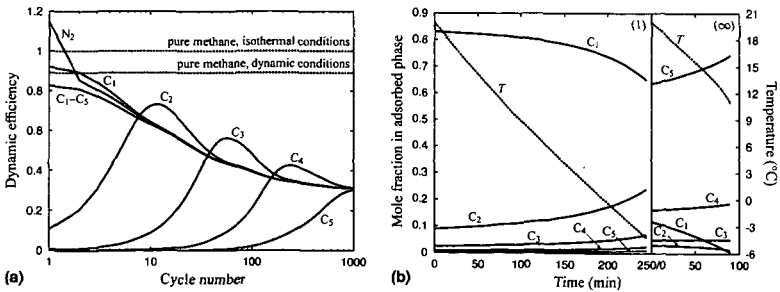


Figure 3: (a) Dynamic efficiency, η_i , as a function of cycle number for an ANG cylinder. (b) Histories of temperature and mole fractions in adsorbed phase for (1) first and (∞) cyclic steady-state discharges in an ANG cylinder.

Block Copolymer Electrolytic Membranes for All Solid-state Rechargeable Lithium Batteries

P.P. Soo, B.Y. Huang, D.R. Sadoway, and A.M. Mayes

Department of Materials Science and Engineering
Massachusetts Institute of Technology
Cambridge, MA 02139-4307

For nearly 20 years, poly(ethylene oxide)-based materials have been researched for use as electrolytes in solid-state rechargeable lithium batteries. Technical obstacles to commercial viability derive from the inability to satisfy simultaneously the electrical and mechanical performance requirements -- high ionic conductivity along with resistance to flow. Here we report the synthesis of poly(lauryl methacrylate)-*b*-poly(oligo(oxyethylene) methacrylate) block copolymer electrolytes in which *both* components have glass-transition temperatures well below room temperature. Microphase separation of the polymer blocks imparts the dimensional stability necessary for thin-film, solid-state battery applications. Electrolytes prepared with these materials display conductivities near 10^{-5} S/cm and are electrochemically stable over a very wide potential window. Cycle testing in prototype batteries demonstrate excellent cyclability and capacity retention.

The lithium solid polymer electrolyte (SPE) battery is arguably the most attractive technology for rechargeable electric power sources, boasting the highest predicted energy density, the fewest environmental, safety and health hazards, low projected materials and processing costs, and greatest freedom in battery configuration. Poly(ethylene oxide) (PEO)-based materials are favored candidates for polymer electrolytes.¹ Although PEO-salt complexes are highly conductive at elevated temperatures ($>10^{-4}$ S cm^{-1} at 70°C), their conductivities drop precipitously at temperatures below the melting point ($T_m = 65^\circ\text{C}$ for PEO). Common strategies to improve conductivity involve modifying the molecular architecture of PEO to suppress crystallization.² While such approaches have resulted in materials whose room-temperature conductivity exceeds 10^{-5} S cm^{-1} , their liquid-like nature typically requires a separator or supporting matrix to allow them to be deployed in a battery configuration. Gel polymer electrolytes combine high ionic conductivity with dimensional stability by infusing a liquid electrolyte into a nonconducting polymer network.^{3,4} However, these systems require suitable packaging of the volatile organics.

Block copolymers offer a novel means to achieve both high ionic conductivity and dimensional stability. These materials consist of two chemically dissimilar polymers covalently bonded end-to-end. At low temperatures or in the absence of solvent, a net repulsion between the polymer blocks induces their local segregation into periodically spaced nanoscale domains. This "microphase separation" event, analogous to crystallization, confers solid-like mechanical properties to the material at macroscopic scales, *even when both polymer blocks are above their respective glass transition temperatures, T_g* .^{5,6} At local scales, however, when $T > T_g$ the mobility

of the polymer chains remains high, even comparable to that in the disordered state.⁷ By choosing an amorphous PEO-based polymer as one block component, continuous ion conducting pathways can be formed in the material upon microphase separation.

For this study, diblock copolymers consisting of a poly(lauryl methacrylate) (PLMA) block ($T_g \sim -40^\circ\text{C}$) and a poly(oligo(oxyethylene) methacrylate) (POEM) block ($T_g \sim -65^\circ\text{C}$) were prepared. POEM employs a PEO side chain with a length of approximately 9 [EO] units, sufficiently low that crystallization does not occur.⁸ The block copolymers were anionically synthesized at -78°C by the sequential addition of lauryl methacrylate (Aldrich) and OEM macromonomer (Polysciences) to a diphenylmethyl potassium initiator in tetrahydrofuran. Upon termination of the reaction with degassed methanol, the copolymer solution was concentrated on a rotary evaporator, precipitated in hexane, and finally centrifuged to isolate the colorless polymer. For comparison purposes, POEM homopolymer was also anionically synthesized following a similar procedure. Molecular weights and compositional characteristics of the polymers are given in Table 1.

Rheological characterization of this system was performed using a Rheometrics ARES rheometer with a parallel plate fixture. The polymer was pressed to a gap width below 1 mm and a stable normal force of approximately 1000 g. The complex shear modulus, $G = G' + iG''$, was then measured as a function of frequency by dynamically shearing the polymer at a fixed strain of 1.5% over the frequency range 0.1 to 250 rad s^{-1} at temperatures from 25°C to 90°C .

Table 1. Molecular weight characteristics of synthesized POEM-based polymers.

	Composition (v:v)	Molecular weight (g/mol)	Polydispersity (M_w/M_n)
PLMA- <i>b</i> -POEM	47:53	64,700	1.1
PLMA- <i>b</i> -POEM	32:68	77,800	1.2
PLMA- <i>b</i> -POEM	23:77	62,900	1.2
POEM	—	100,000	1.3

The rheological behavior of block copolymer varies dramatically depending on whether the material resides in the ordered or disordered state. In the PLMA-*b*-POEM block copolymers, the storage modulus reaches a plateau value at low frequencies while the loss modulus assumes a limiting power law in which $G'' \sim \omega^{0.5}$. This low-frequency scaling behavior is characteristic of a microphase-separated system,⁵ and verifies its solid-like nature. Even after blending with significant amounts (23 wt%) of poly(ethylene glycol) dimethyl ether (PEGDME, Polysciences, $M=430 \text{ g mol}^{-1}$), the low-frequency scaling behavior is preserved, indicating that these short PEO chains stay confined to the POEM domains of the copolymer morphology. The formation of nanoscale domains was further verified by direct imaging with transmission electron microscopy. By contrast, the POEM homopolymer exhibits the low frequency scaling behavior $G'' \sim \omega$, indicative of a polymer in its molten state.

Conductivity measurements were performed on the POEM homopolymer and the PLMA-*b*-POEM block copolymers at fixed salt concentration $[\text{EO}]:\text{Li}^+ = 20:1$. Specimens for

conductivity measurements were initially dried in a vacuum oven at 70°C for 24 hours. LiCF_3SO_3 (lithium triflate) was dried *in vacuo* at 130°C for 24 hours. The materials were then transferred to an inert atmosphere, dissolved in dry THF, and solution cast on a glass die. The polymer/salt complex was then annealed *in vacuo* for 48 hours at 70°C. Under dry nitrogen, the polymer electrolyte was loaded between a pair of blocking electrodes made of type 316 stainless steel, pressed to a thickness of 250 μm , and annealed *in situ* at 70°C for 24 hours. Over the temperature interval spanning -20°C to 90°C electrical conductivity was measured by impedance spectroscopy using a Solartron 1260 Impedance Gain/Phase Analyzer.

Figure 1 illustrates that at room temperature the doped 32:68 PLMA-*b*-POEM block copolymer displays ionic conductivities similar to that of pure POEM. As expected, increasing the POEM content of the copolymer had the effect of increasing conductivity. Significantly higher conductivities were achieved by blending the block copolymer with 23 wt% PEGDME, resulting in σ values exceeding $10^{-5} \text{ S cm}^{-1}$ at room temperature.

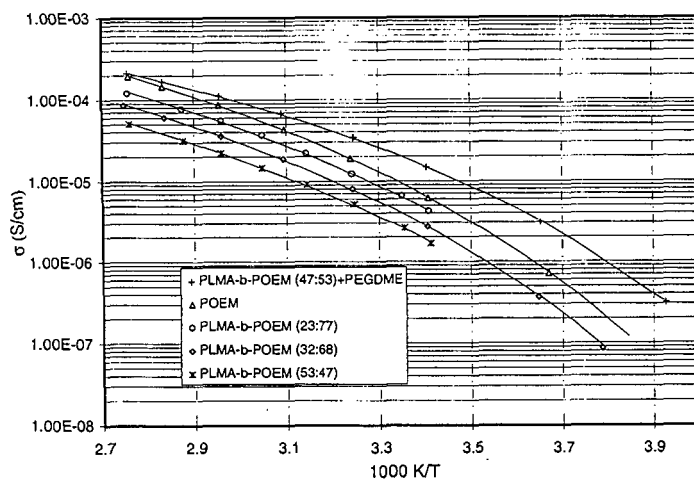


Figure 1. Compositional dependence of conductivity in PLMA-*b*-POEM diblock copolymers doped with LiCF_3SO_3 ([EO]: Li^+ = 20:1).

Cyclic voltammetry was performed on a block copolymer electrolyte (BCE) composed of 87 wt% 32:68 PLMA-*b*-POEM and 23 wt% PEGDME at a salt concentration of [EO]: LiCF_3SO_3 = 20:1 to investigate the range of electrochemical stability of the material. Films were prepared under an inert atmosphere by casting the BCE onto lithium foil from dry THF solution. The resulting films were placed under vacuum at room temperature overnight to remove excess solvent. The BCE was sandwiched between a counter electrode of lithium and a working electrode of aluminum, with a film thickness of approximately 150 μm . A lithium reference electrode was extruded into the cell through the side and positioned near the working electrode. Using a 1286 Solartron Electrochemical Interface, potential was scanned from +2.0 to +5.0 V vs. Li/Li^+ at a sweep rate of 0.5 mV s^{-1} . Current levels below 0.6 $\mu\text{A cm}^{-2}$ were measured between

2.0 and 5.0 V, indicating that the material is electrochemically stable over this voltage interval, which brackets that used in commercial lithium-ion batteries.

The composite cathode of the solid-state battery was prepared by casting a suspension of a mixture of $\text{LiAl}_{0.25}\text{Mn}_{0.75}\text{O}_2$ (45 wt%), carbon black (7 wt%), graphite (6 wt%), and BCE (42%) in dry THF solution onto an Al foil heated to 60°C. Evaporation of the THF produced a cathode film ~150 μm in thickness. The resulting cathode film was placed under vacuum for 48 hours at 60°C to remove any moisture present. This material was cut into square electrodes measuring 1 cm on a side. The $\text{LiAl}_{0.25}\text{Mn}_{0.75}\text{O}_2$ powder, which serves as the intercalation compound in the cathode, was produced by co-precipitation of hydroxides followed by firing in air at 945°C. Details of oxide synthesis and characterization are published elsewhere¹². The $\text{Li}/\text{BCE}/\text{LiAl}_{0.25}\text{Mn}_{0.75}\text{O}_2$ solid state battery was then fabricated by laminating lithium metal, BCE, and the composite cathode film containing $\text{LiAl}_{0.25}\text{Mn}_{0.75}\text{O}_2$ together in an argon-filled glove box. Cycle testing was conducted between 2.0 and 4.4 V with a MACCOR Series 4000 Automated Test System at a current density of 0.05 mA cm^{-2} .

Room temperature cycle testing of the $\text{Li}/\text{BCE}/\text{LiAl}_{0.25}\text{Mn}_{0.75}\text{O}_2\text{-C-BCE}$ cell is shown in figure 2. Fig. 2(a) shows the first cycle which begins with lithium removal from $\text{LiAl}_{0.25}\text{Mn}_{0.75}\text{O}_2$ over the voltage range spanning 3.0 to 4.4 V. A single charging plateau at ~3.6 V is observed, and the initial charging capacity was found to be 136 mAh/g . The first discharge exhibited a capacity of 108 mAh/g and featured the emergence of two voltage steps, one at ~4.0 V and another at ~3.0 V, indicating lithium intercalation at two distinct sites. This behavior is characteristic of the spinel phase $\text{Li}_x\text{Mn}_2\text{O}_4$ for which it is reported that the 3.0 V plateau corresponds to lithium insertion into octahedral sites and the 4.0 V plateau corresponds to lithium

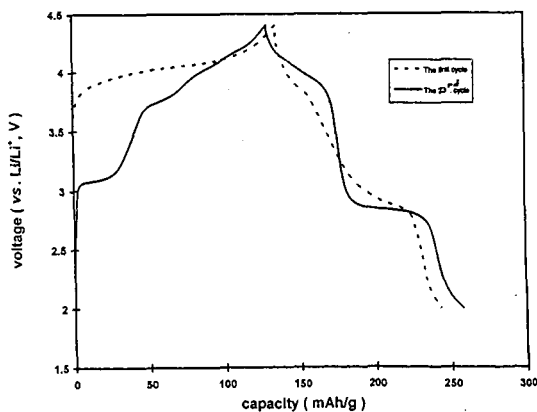


Figure 2. Charge/discharge cycling of the $\text{LiAl}_{0.25}\text{Mn}_{0.75}\text{O}_2/\text{BCE}/\text{Li}$ cell with a current density of 0.05 mA/cm^2 cycled between 2.0 and 4.4 V. (a) first cycle; (b) 23rd cycle.

insertion into tetrahedral sites.¹³ After further cycling, the voltage steps became more distinct as can be seen in Fig. 2(b), which shows the 23rd cycle. After ~12 cycles, the intercalation oxide reached its optimal capacity of ~125 mAh/g . This result indicates that the cell has demonstrated

good cyclability when cycled over both 4.0 V and 3.0 V plateaus. Further discussion of the oxide characteristics is reported in a separate manuscript.¹²

Although several groups had previously investigated PEO-based block copolymers as candidate electrolytes for rechargeable Li batteries,⁹⁻¹¹ the conductivities and temperature window of operation of those materials were not optimized because one block component either crystallized or underwent a glass transition above room temperature. Here we demonstrate that by joining two non-crystallizing polymers with T_g s well below 0°C, a dimensionally stable electrolyte can be prepared with conductivities near that of the POEM homopolymer. We expect that moving to block components with higher room temperature conductivities and/or lower glass transitions should further improve both the ambient temperature performance and temperature window of operation.

Acknowledgments

This project has been funded by Furukawa Electric Co., Ltd. and by the INEEL University Research Consortium. We are thankful to Y.-I. Jang and Y.M. Chiang for providing cathode materials. The technical assistance of M.J. Fasolka, M.E. King, M. Nakajima, and Y.-I. Jang is also gratefully acknowledged as are helpful discussions with Professors G. Ceder and Y.-M. Chiang.

References

1. Armand, M.B. *Polymer Electrolyte Reviews* **1**, Ch. 1 (1987).
2. Gray, F.M. *Solid Polymer Electrolytes: Fundamentals and Technological Applications*, Ch. 6 (VCH Publishers, New York, 1991).
3. Scrosati, B. (ed.) *Applications of Electroactive Polymers* (Chapman and Hall, London, 1993).
4. Abraham, K.M. and Jiang, Z. *J. Electrochem. Soc.* **144**, 1136 (1997).
5. Bates, F.S. *Macromolecules* **17**, 2607 (1984); Rosedale, J.H. and Bates, F.S. *Macromolecules* **23**, 2329 (1990).
6. Russell, T.P., Karis, T.E., Gallot, Y. and Mayes, A.M. *Nature* **368**, 729 (1994).
7. Ehlich, D., Takenaka, M. and Hashimoto, T. *Macromolecules* **26**, 492 (1995).
8. Yan, F., Dejardin, P., Frere, Y. and Gramain, P. *Makromol. Chem.* **191**, 1197 (1990).
9. Gray, F.M., MacCallum, J.R., Giles, J.M., and Vincent, C.A., *Macromolecules* **21**, 392 (1988).
10. Khan, I.M., Fish, D., Delaviz, Y. and Smid, J. *Makromol. Chem.* **190**, 1069 (1989).
11. Lobitz, P., Reiche, A. and Fullbier, H. *J. Power Sources* **43**, 467 (1993).
12. Y.I. Jang, B.Y. Huang, Y.M. Chiang, and D.R. Sadoway, *J. Electrochem. Soc.*, in press.
13. M.M. Thackeray, W.I.F. David, P.G. Bruce, and J.B. Goodenough, *Mat. Res. Bull.*, **18**, 461 (1983).